NAVAL POSTGRADUATE SCHOOL

MONTEREY, CALIFORNIA

THESIS

INVESTIGATING THE CHARACTERISTICS OF THE SOUTHERN BEAUFORT SEA USING ACOUSTICAL OCEANOGRAPHY SENSORS DURING ICEX-18

by

Jeffrey D. Collins II

March 2019

Thesis Advisor: John E. Joseph
Co-Advisor: Davis B. Reeder

THIS PAGE INTENTIONALLY LEFT BLANK

REPORT DOCUMENTATION PAGE	*Form Approved OMB No. 0704-0188*

1. AGENCY USE ONLY *(Leave blank)*	**2. REPORT DATE** March 2019	**3. REPORT TYPE AND DATES COVERED** Master's thesis

4. TITLE AND SUBTITLE
INVESTIGATING THE CHARACTERISTICS OF THE SOUTHERN BEAUFORT SEA USING ACOUSTICAL OCEANOGRAPHY SENSORS DURING ICEX-18

5. FUNDING NUMBERS
RCM04

6. AUTHOR(S) Jeffrey D. Collins II

7. PERFORMING ORGANIZATION NAME(S) AND ADDRESS(ES)
Naval Postgraduate School
Monterey, CA 93943-5000

8. PERFORMING ORGANIZATION REPORT NUMBER

9. SPONSORING / MONITORING AGENCY NAME(S) AND ADDRESS(ES)
N/A

10. SPONSORING / MONITORING AGENCY REPORT NUMBER

11. SUPPLEMENTARY NOTES The views expressed in this thesis are those of the author and do not reflect the official policy or position of the Department of Defense or the U.S. Government.

12a. DISTRIBUTION / AVAILABILITY STATEMENT
Approved for public release. Distribution is unlimited.

12b. DISTRIBUTION CODE
A

13. ABSTRACT (maximum 200 words)

During Ice Exercise (ICEX) 2018, a 120-kHz echosounder was used to investigate the ocean environment underneath the Arctic ice sheet in the southern Beaufort Sea down to a depth of 200 meters. Returns from the echosounder, coupled with data from an Acoustic Doppler Current Profiler (ADCP) and a Conductivity, Temperature, and Depth (CTD) profiler, suggest the presence of sharp, sound-speed gradients throughout the water column, occurring more often at greater depths. The pattern of returns can be correlated to variations in temperature and salinity common to the development of microstructure, suggesting a mechanism related to the formation of thermohaline staircases at greater depths. The presence of microstructure at shallower depths provides a potential source of detection of submerged objects via their hydrodynamic signature resulting from the disturbance of the microstructure. The current profile from the ADCP, along with the movement of the ice floe, provides evidence of shear at a depth near 20 meters, which allows for water from the lower, warmer mass to penetrate upwards toward the ice, increasing the vertical heat flux and impacting the melting of ice.

14. SUBJECT TERMS
acoustical oceanography, acoustic scattering, ADCP, Arctic, Beaufort Sea, echosounder, ICEX, microstructure

15. NUMBER OF PAGES
65

16. PRICE CODE

17. SECURITY CLASSIFICATION OF REPORT	**18. SECURITY CLASSIFICATION OF THIS PAGE**	**19. SECURITY CLASSIFICATION OF ABSTRACT**	**20. LIMITATION OF ABSTRACT**
Unclassified	Unclassified	Unclassified	UU

NSN 7540-01-280-5500

Standard Form 298 (Rev. 2-89)
Prescribed by ANSI Std. 239-18

THIS PAGE INTENTIONALLY LEFT BLANK

Approved for public release. Distribution is unlimited.

INVESTIGATING THE CHARACTERISTICS OF THE SOUTHERN BEAUFORT SEA USING ACOUSTICAL OCEANOGRAPHY SENSORS DURING ICEX-18

Jeffrey D. Collins II
Lieutenant, United States Navy
BS, U.S. Naval Academy, 2012

Submitted in partial fulfillment of the
requirements for the degree of

MASTER OF SCIENCE IN PHYSICAL OCEANOGRAPHY

from the

NAVAL POSTGRADUATE SCHOOL
March 2019

Approved by: John E. Joseph
Advisor

Davis B. Reeder
Co-Advisor

Peter C. Chu
Chair, Department of Oceanography

THIS PAGE INTENTIONALLY LEFT BLANK

ABSTRACT

During Ice Exercise (ICEX) 2018, a 120-kHz echosounder was used to investigate the ocean environment underneath the Arctic ice sheet in the southern Beaufort Sea down to a depth of 200 meters. Returns from the echosounder, coupled with data from an Acoustic Doppler Current Profiler (ADCP) and a Conductivity, Temperature, and Depth (CTD) profiler, suggest the presence of sharp, sound-speed gradients throughout the water column, occurring more often at greater depths. The pattern of returns can be correlated to variations in temperature and salinity common to the development of microstructure, suggesting a mechanism related to the formation of thermohaline staircases at greater depths. The presence of microstructure at shallower depths provides a potential source of detection of submerged objects via their hydrodynamic signature resulting from the disturbance of the microstructure. The current profile from the ADCP, along with the movement of the ice floe, provides evidence of shear at a depth near 20 meters, which allows for water from the lower, warmer mass to penetrate upwards toward the ice, increasing the vertical heat flux and impacting the melting of ice.

THIS PAGE INTENTIONALLY LEFT BLANK

TABLE OF CONTENTS

LIST OF FIGURES

LIST OF ACRONYMS AND ABBREVIATIONS

3D	three-dimensional
ADCP	Acoustic Doppler Current Profiler
AIWEX	Arctic Internal Wave Experiment
APL-UW	Applied Physics Laboratory-University of Washington
CTD	Conductivity, Temperature, and Depth
DSL	deep scattering layer
EL	echo level
GDEM	Generalized Digital Environmental Model
GSW	Gibbs-SeaWater
ICEX	Ice Exercise
ITP	Ice-Tethered Profilers
MAVS	Modular Acoustic Velocity Sensor
mS	millisiemens
NaN	Not-a-Number
NPS	Naval Postgraduate School
NSTM	near-surface temperature maximum
PSL	pycnocline scattering layer
PSU	practical salinity unit
PSW	Pacific Summer Water
PWW	Pacific Winter Water
rms	root mean square
S	Siemens
SASC	Senate Armed Services Committee
SL	source level
SSP	sound speed profile
TDA	tactical decision aid
TS	target strength
TL	transmission loss
USNORTHCOM	U.S. Northern Command
VLA	vertical line array
XBT	Expendable Bathythermograph

THIS PAGE INTENTIONALLY LEFT BLANK

ACKNOWLEDGMENTS

First and foremost, I want to thank God, my Creator, Sustainer, and Redeemer for the many blessings He has placed in my life. The ability to research the mysteries of His creation and pursue new discoveries is a testament of His all-knowing and all-powerful nature. Studying the mechanics of His creation is an awesome and humbling experience.

I want to thank my parents and the rest of my family for their continued love and support. They have always encouraged me to pursue my goals, and have provided invaluable wisdom and guidance throughout my career.

I want to thank my advisors, John Joseph and Ben Reeder. I appreciate your willingness to take me onboard for this research. Your passion and knowledge in the field of acoustics and the Arctic is contagious and provided motivation to me throughout the research process. Your feedback and questions helped keep me honest in my statements and provided experienced guidance in the process of scientific writing.

I want to thank RADM Ellis and RDML Williams for the resources and support they provided to me as a member of the Undersea Warfare program. They, along with CDR Travis, Bard Mansager, and Laurie Sheehan, supported me immensely, allowing me to make the most of my NPS experience.

I want to thank all of my professors who took the time to impart the knowledge of their subjects on me. They provided the many pieces necessary to help build this research to the final product. Special thanks to Mike Cook for your MATLAB expertise and our Monday Morning Quarterback sessions.

I want to thank the members of the Marina Church of Christ for welcoming me into your family, and for allowing me the opportunity to grow and serve the Lord with you.

Finally, I want to thank the members of JCASL for providing a dose of humor, witty banter, and good company every Thursday afternoon in the Rose Garden.

THIS PAGE INTENTIONALLY LEFT BLANK

I. INTRODUCTION

A. ARCTIC

The Arctic Ocean remains a frontier for exploration to the present day. It presents a set of unique oceanographic and acoustic properties because of its combination of ice cover and near-uniform cold-water temperature. Expanding our knowledge about the Arctic occurs at a relatively slow pace because of the extreme environmental factors that preclude prolonged field experiments in the region. However, with the decrease in sea ice over time, the Arctic Ocean will become more accessible to both surface and sub-surface traffic from nations throughout the region. This increase in accessibility will drive world leaders to pay closer attention to activity in the Arctic, home of an abundance of natural resources and wildlife habitats. Additionally, unhindered travel through the Arctic Ocean would reduce travel time and cost for merchants traversing between the Atlantic and Pacific Oceans. This equates to lucrative potential for many types of businesses.

Many of the highest-ranking officials in the U.S. military and government made have statements over the past of couple years regarding the importance of the Arctic region and the essential security role the United States must take in the region. In her 2018 U.S. Northern Command (USNORTHCOM) posture statement before the Senate Armed Services Committee (SASC), GEN Robinson conveyed the importance of conducting exercises in the region to better understand the requirements for operating in the Arctic in order to "support domain awareness, communications, infrastructure, and a sustainable presence (Robinson 2018)." In his *National Security Strategy*, President Trump singled out the Arctic as its own domain, alongside land, sea, outer space, and the digital realm, in discussing the importance of maintaining the established rules of order when operating within each domain (Trump 2017). With the attention of our government and military leaders, the Arctic remains a vital area for scientific research, technological advancement, and most importantly, a key focus for our national defense posture.

B. MOTIVATION

As technological advances in weaponry and platforms continue to narrow the tactical-advantage gap between ourselves and other nations, the ability to understand the environment that we operate in and capitalize on that knowledge to our advantage becomes more crucial than ever before. Traditionally, the tactical decision aids (TDA) utilized by our forces for acoustic detection implement oceanographic models consisting of climatological values resulting in sound speed profiles (SSP) with a monotonic increase with depth as shown in Figure 1. Field experimentation focused on the hydrodynamics and acoustic properties of the Arctic Ocean sheds light on the environment's phenomena that impact our ability to exploit the characteristics of the region.

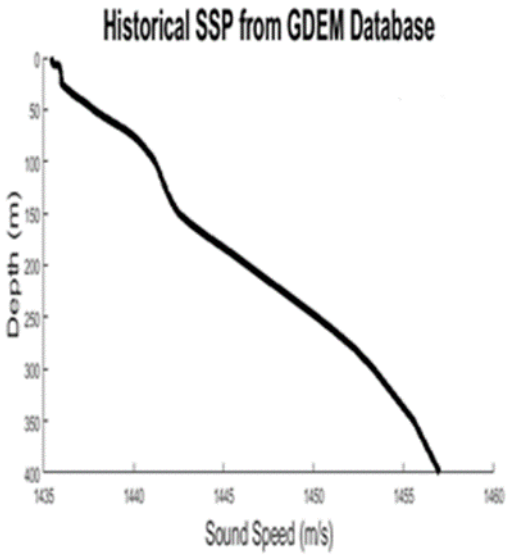

Figure 1. Standard Climatology Sound Speed Profile in the Arctic Ocean.
Adapted from Nelson (2016).

The research team designed the field experiment to examine the effectiveness of a high-frequency echosounder in mapping the fine structure underneath the ice sheet with the goal of providing further insight on significant-ocean variability observed at the interface of the surface layer and Pacific Summer Water (PSW) during ICEX 2016 as depicted in Figure 2.

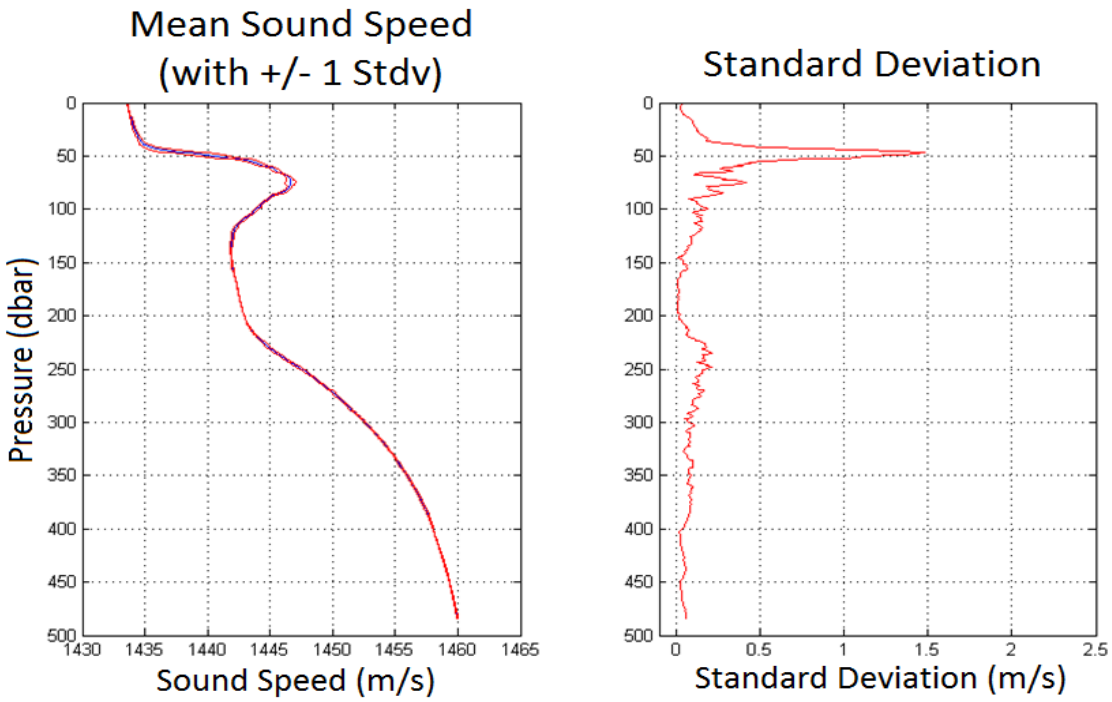

The graph on the left represents the mean sound speed profile in blue and +/- 1 standard deviation from the 7 CTD casts shown in red. The graph on the right highlights the variability identified at 50 meters.

Figure 2. Comparison of Sound Speed Profiles with Standard Deviation.
Source: Nelson (2016).

It is immediately apparent from only a cursory look at Figures 1 and 2 that climatological data used in our TDAs are not capturing the significant ocean and acoustic variability within the water column near depths closely associated with the mixed layer and PSW interface. Through continued field research, we aim to broaden our understanding of this variability and the impact of the interface on acoustics. With more knowledge regarding the extent and occurrence of this acoustic variability, we desire to demonstrate the need for this variability to be incorporated into our fleet's TDAs and operational decision making. This research examines the environment underneath the Arctic ice through the lenses of multiple types of instruments with the goal of clearly identifying the presence and magnitude of the oceanographic and acoustic variability while providing possible explanations for the variability and ways to exploit this knowledge to our tactical advantage.

THIS PAGE INTENTIONALLY LEFT BLANK

II. BACKGROUND/THEORY

A. THE BEAUFORT SEA

The Beaufort Sea is located within the Canadian Basin of the Arctic Ocean directly north of Alaska, Yukon Territory, and Northwest Territories. Its surface circulation is dominated by the Beaufort Gyre, an anticyclonic circulation dictating both water and ice motion, while its deep circulation below 200 meters is cyclonic (Talley et al. 2011). Along the Alaskan and Canadian coast, the Alaskan Coastal Current, a rim current, branches from the Bering Strait inflow providing warm, Pacific Ocean water and runs opposite the direction of circulation of the Beaufort Gyre (Talley et al. 2011). Underneath the ice cover, the Beaufort Sea consists of multiple water masses originating in the Arctic, Atlantic, and Pacific oceans as shown in Figure 3. Each water mass possesses its own unique characteristics and their interactions impact the temperature, salinity, and sound speed profiles of the Beaufort Sea. Additionally, while not conducive to long-term human inhabitance, the Beaufort Sea is home to a variety of fish and other microorganisms. Both the characteristics of the water masses and the biological presence contained within the Beaufort Sea are examined further in the following sections.

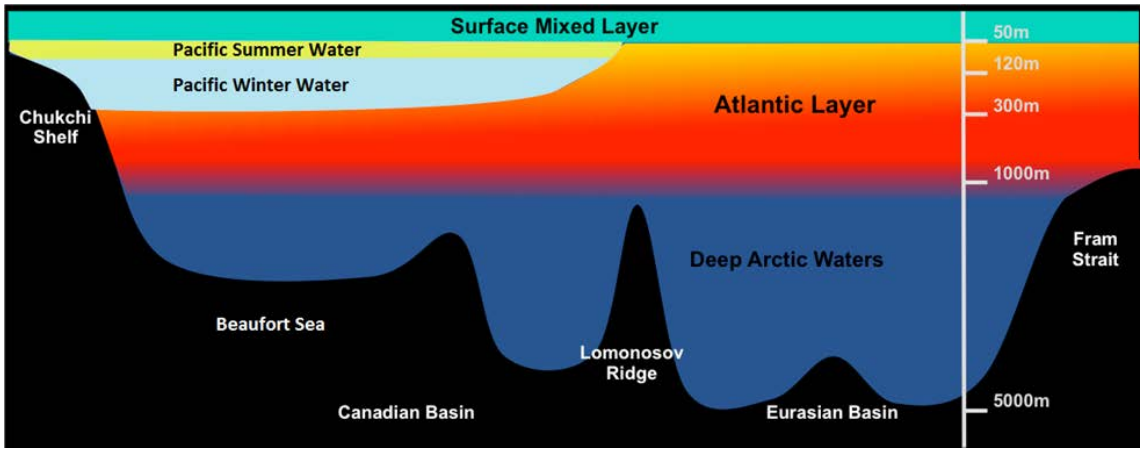

Figure 3. Cross Section of Water Mass in Arctic Ocean. Adapted from DiMaggio (2016).

1. Hydrography

The surface mixed layer exists across the entire Arctic Ocean, and it extends from the surface to a depth ranging between 25–50 m (Talley et al. 2011). The temperature and salinity of the mixed layer is strongly controlled by the freezing or melting of ice, maintaining the values within a range between -1.8°C and -1.5°C and from 28 to 33.5 practical salinity units (PSU), respectively (Talley et al. 2011). Below the mixed layer in the Canadian basin, summer and winter water from the Pacific Ocean, entering through the one-way Bering Strait inflow, provide more complicated vertical and horizontal structures than the ones found within the Eurasian Basin (Talley et al. 2011). The PSW creates a temperature maximum supported by a strong halocline at a depth approximately 50 to 100 m beneath the mixed layer (Talley et al. 2011). An analysis of data collected from Ice-Tethered Profilers (ITP), moorings, and hydrographic surveys between 2003 and 2013 led Timmermans et al. (2014) to conclude the PSW layer is thickening, warming, and freshening, as well as demonstrating spatial and temporal variability. Additionally, Jackson et al. (2010) demonstrated the shoaling and warming of the near-surface temperature maximum (NSTM) by 2.1 m/yr from 2004 to 2007 and 0.13 °C/yr from 1997 to 2007, respectively. This variability poses significant implications for sea-ice extent and acoustic propagation.

Below the PSW, the Pacific Winter Water (PWW) presents a temperature minimum at an approximate depth of 150 m (Talley et al. 2011). Below the PWW, the temperature continues to increase with depth until reaching the maximum in the Atlantic layer, ranging between depths of 200 to 900 m (Talley et al. 2011). According to Turner (2010), there is enough heat stored in the Atlantic layer, if allowed to flux upward to interact with the ice at a rate of 6.7 W m^{-2} or 2.1 X 10^{8} J m^{-2} yr^{-1}, to melt all of the ice, with a mean thickness of 2.5 m, in four years. The majority of this heat content is subdued underneath the halocline, but double-diffusive convection, also known as thermohaline staircases, is a possible mechanism for heat flux through the halocline (Turner 2010). Thermohaline staircases are discussed further in Section B of this chapter.

2. Biological Presence

While not as densely populated as other oceans, the Arctic Ocean is home to a variety of biological organisms, ranging from algae under the ice, plankton, jellyfish, several species of fish, and whales (Ashjian 2004). While not immensely significant to the hydrodynamics of the Arctic Ocean, the mention of the biological presence within the Beaufort Sea is relevant to this study due to the connection with the field of fishery acoustics. Fishery acoustics works include the study of many of the inhabitants of the Arctic and the notable returns often observed in echosounder data from biological organisms. Equipped with the knowledge of the biological organisms present in the Arctic Ocean, referencing Holliday and Pieper (1980), Simmonds and MacLennan (2005), and McBride et al. (2014) to determine typical target strength (TS) values of fish and plankton will assist in the determination of the cause of returns in the echosounder data.

B. THERMOHALINE STAIRCASES

Thermohaline staircases are a hydrodynamic phenomenon occurring over a horizontal extent covering 80% of the Canadian Basin, and occurring at depths ranging from 150–300 m with layer thicknesses in the range of 0.5 m–3.5 m throughout the Arctic Ocean (Shibley et al. 2017). This depth is approximately 100 m shallower compared to the Arctic Internal Wave Experiment (AIWEX) measurements in 1985 (Radko 2013). It is commonly accepted that a link exists between thermohaline staircases and double-diffusive convection, when salinity and temperature gradients share the same sign (Turner 1965). Typical profiles that the namesake of this phenomenon is derived are shown in Figure 4. Despite the commonly accepted link between the two, there still remains a debate regarding the underlying mechanism causing the formation of the thermohaline staircases (Radko 2013). These theories include collective instability, thermohaline intrusions that develop into a staircase, metastable equilibria initially forced by external disturbances, applied flux mechanism, negative-density diffusion, and instabilities of the flux-gradient laws followed by a series of mergers (Radko 2013). Recent modeling of thermohaline-staircase regeneration following their disruption caused by a submersible object suggests a window of opportunity for detection of the submersible by monitoring the state of the staircases

(Davis 2018). In the modeling, Davis (2018) examined two, separate, regeneration regimes, double-diffusion and one termed “mechanical regeneration.” With the continued debate of the origin of thermohaline staircases and the new modeling study suggesting submersible-detection capabilities, further field studies of the mechanics of thermohaline staircases are vitally important. This study attempts to take the next step in the form of an in-situ experiment utilizing an echosounder to map the environment underneath the ice down to a depth of 200 meters, with the goal of providing evidence of fine structure detectable by an echosounder.

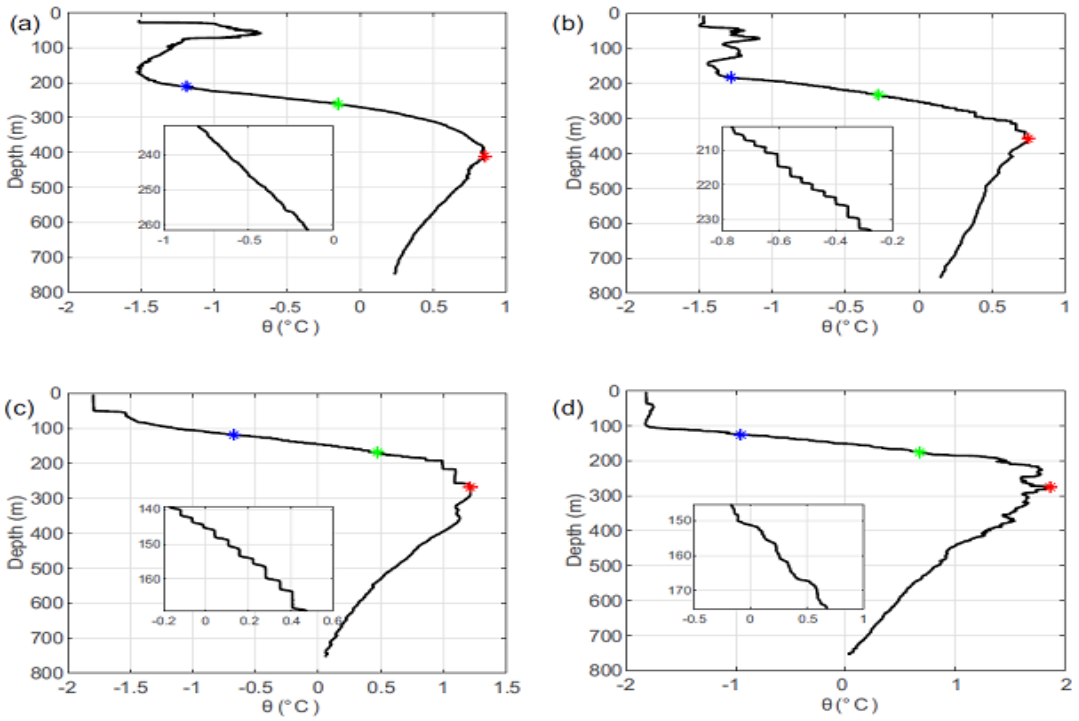

Note: (a) Profile from Canadian Basin boundary, (b) profile from central Canadian Basin, (c) profile from the Eurasian Basin, (d) profile from the vicinity of Fram Strait. Blue and green stars represent the shallow and deep bounds of the inset, respectively. Red stars represent the Atlantic Water Layer potential temperature maximum.

Figure 4. Typical Staircase Profiles in the Arctic Ocean. Source: Shibley et al. (2017).

C. ACOUSTIC FUNDAMENTALS

1. Active-Sonar Equation

The traditional active-sonar equation in a noise background is given in Urick (1983) as

$$SL - 2TL + TS = NL - DI + DT, \tag{1}$$

where SL is source level, TL is transmission loss, TS is target strength, NL is noise level, DI is directivity index, and DT is detection threshold, all in units of dB re 1 μPa. The left side of the equation is commonly referred to as the echo level (EL), a measure of the intensity of the echo in the water at the hydrophone. The right side of the equation in commonly referred to as the noise-masking level or minimum-detectable echo level. When both sides of the equation are equal, there will be no detection at the hydrophone. When the EL is larger than the noise-masking level, called echo excess, detection is possible. The variables in the active-sonar equation can be arranged in a number of combinations that provide measures of a sonar-systems performance. It is of importance to note the definition provided by Urick (1983) regarding the variables in the sonar equation used a reference distance of 1 yard because, at the time of publication of his first edition, the unit of yard was still frequently used in acoustics. However, since that time, the acoustics community has transitioned to the metric system, using the reference distance of 1 meter instead. Urick (1983) provides a correction for using these variables in metric units in the sonar equation by reducing their values by 0.78 dB.

1. Source Level

Source level (SL) provides a measure of the acoustic output of a given source. Urick (1983) defines SL as "the intensity of the radiated sound in decibels relative to the intensity of a plane wave of [root mean square] (rms) pressure 1μPa, referred to a point 1 yard from the acoustic center of the projector in the direction of the target." An equation for the SL of an omnidirectional source as a function of power is given by

$$SL = 171.5 + 10 \log P, \tag{2}$$

where P is power in watts (Urick 1983).

2. Transmission Loss

Transmission loss (TL) can be modeled in a spherical or cylindrical shape depending on the environmental layout that the sound is being propagated. Cylindrical spreading occurs when the sound propagation is bounded by two-parallel planes, whereas spherical spreading is appropriate when the sound has a free field to propagate through. Typically, in an experiment transmitting from the surface in the downward direction without a shallow bottom, the equation for one-way TL is

$$TL = 20 \log r, \tag{3}$$

where r is the range in meters between the source and the target (Urick 1983). However, because the ice sheet presents an upper, reflective boundary and upward refraction is common, it is discussed in Urick (1983) that transmission loss in the horizontal is less than the spherical model at short ranges, such as the 400 meters maximum two-way transmission range in this experiment. Therefore, if transmission loss were being modeled within this study, it would be appropriate to use a transmission-loss calculation in between the cylindrical and spherical spreading models.

3. Target Strength

TS is a measure of the echo returned by an object, which ranges from submarines, mines, fish, or plankton. Urick (1983) defines TS, in the context of the active-sonar equations, as “10 times the logarithm to the base 10 of the ratio of the intensity of the sound returned by the target, at a distance of 1 yard from its “acoustic center” in some direction, to the incident intensity from a distant source.” TS depends considerably on the frequency and orientation relative to the source, material properties, size, and shape of the object reflecting the incident sound. The generic equation for TS is given by Urick (1983) as

$$TS = 10 \log \left. \frac{I_r}{I_i} \right|_{r=1}, \tag{4}$$

where I_r is the intensity of return at 1 yard, and I_i is the incident intensity.

D. ACOUSTIC SCATTERING

1. Echosounders

Echosounders entered the field of ocean acoustics as a tool for measuring volume scatterers as far back as the 1950s, with their use in observing plankton during the study of Cushing and Richardson (1956). A few years later in 1962, echosounders were used to observe internal waves using frequencies ranging from 5- to 25-kHz (Proni and Apel 1975). Echosounders gained commercial notoriety as instruments for fishermen, commonly referred to as fish-finders. Throughout the years, echosounders and similar acoustic-backscattering techniques have been used scientifically to study zooplankton (Holliday and Pieper 1980), fish (Reeder et al. 2004), and ocean microstructure (Lavery et al. 2003). More recently, a commercially-available Simrad EK80 broadband (15–25 kHz) echosounder was deployed on icebreaker *Oden* to map thermohaline staircases in the Arctic during the summer of 2016 (Stranne et al. 2017). The characteristics of the echosounder used during ICEX-18 are discussed in Chapter III, Section C.

2. Volume Scattering

An echosounder relies on volume scattering to map out various characteristics of the ocean environment to include biological organisms and the ocean bottom. The equation for both surface and volume scattering strength looks similar to that of TS, and it is given in Urick (1983) as

$$S_{s,v} = 10 \log \frac{I_{scat}}{I_{inc}}, \tag{5}$$

where I_{scat} is the intensity of the sound scattered by an area of 1 yd^2 or a volume of 1 yd^3, when the intensity is measured at a greater distance and reduced to 1 yd, and I_{inc} is the intensity of the incident plane wave. According to Urick (1983), typically, volume scatterers are spread irregularly throughout the water column, but occasionally these scatterers will lie in finite layers and act as surface scatterers, such as in the deep scattering layer (DSL). Additionally, the DSL is found at depths between 180 and 900 meters during the day, and it tends to be shallower at night. He also described the DSL as showing little

to no variation of scattering strength with frequencies in excess of 20 kHz, and that with a frequency of 24 kHz, the scattering strength of the DSL ranged between -70 to -90 dB. However, in the Arctic Ocean, the DSL is no longer considered “deep” because it is found just beneath the ice cover (Hansen and Dunbar 1970).

In March 1967, the Lamont-Doherty Geological Observatory installed a 100-kHz Ross Model 200A Fineline echosounder on the ice island known as T-3 (Hansen et al. 1971). With this echosounder they observed a thin, shallow scattering layer at approximately 50 meters that correlated to the boundary between the upper Arctic water and the Pacific-water layer beneath (Hansen et al. 1971). This scattering layer became known as the pycnocline scattering layer (PSL) (Hansen et al. 1971). Hansen et al. (1971) found the cause of the scattering return at the PSL is the presence of cosmopolitan thecosomatous pteropod *Spiratella helicina* at the interface between the two water masses, which they confirmed though the collection of the plankton in nets during the experiment. This knowledge of volume scattering and the PSL is utilized in the analysis of the ICEX-18 echosounder data.

III. EXPERIMENTAL DESIGN

A. ICEX-18

Ice Camp SKATE located in the southern Beaufort Sea served as the headquarters for ICEX-18. Due to weather and scheduling conflicts, the Naval Postgraduate School (NPS) field-experiment team was only afforded a narrow window of time on March 9, 2016 to conduct their fieldwork. The team cleared out a set of previously-drilled holes in a cloverleaf pattern to deploy the echosounder's digital transducer and the Acoustic Doppler Current Profiler (ADCP). The team attached the echosounder's digital transducer to a metal plate suspended from a nylon line to a depth of two meters putting the transducer below the 1-meter-thick ice. The line was wrapped around a metal pole laid across the opening of the hole in the ice and moved to one end of the cloverleaf pattern. On the opposite end of the cloverleaf, the ADCP connected to a 2-meter chain suspended from the same type of metal pole laid across the ice hole. Following the deployment of the first-two instruments, the team drilled a 10-inch hole in the ice sheet near the camp with an auger through which the Conductivity, Temperature, and Depth (CTD) profilers and Acousonde recorders were deployed. The CTDs and Acousonde recorders were deployed approximately an hour later on a 5/16-inch Spectra line with a small weight attached to the end of the line to provide negative buoyancy. The CTDs were attached at depths of 40 and 100 meters, and the Acousonde recorders were attached at depths of 25, 50, and 150 meters. A more-thorough description of the equipment specifications is presented in Section C of this chapter. All equipment was collected at the completion of the field research, and all data processing and analysis occurred at NPS.

B. ICEX-16

NPS participated in ICEX-16 from March 10, 2016 to March 12, 2016. According to Nelson (2016), Acousonde recorders were deployed at depths of 30 and 183 meters on vertical line arrays (VLA) positioned 1.25 and 2.83 kilometers away from the G34 acoustic source with 160 degrees of separation between the VLAs referenced from the source. The Acousonde recorders captured acoustic transmissions above, below, and across the

anticipated sound velocity peak at 50 meters (Nelson 2016). A comparison of the locations of data collection for ICEX-16 and ICEX-18 is displayed in Figure 5.

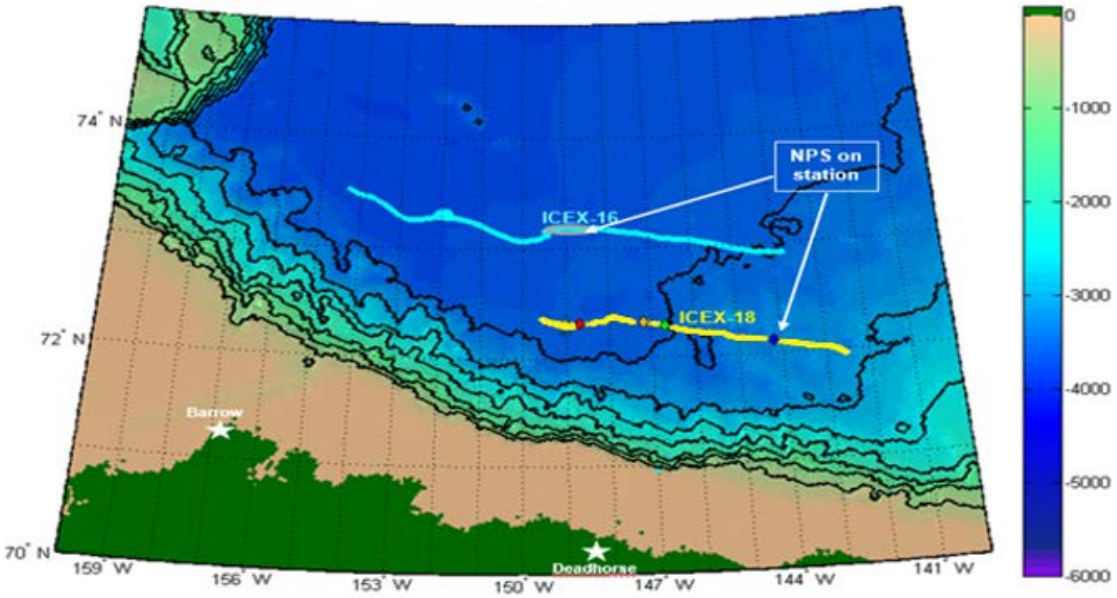

Note: Contour interval of 500 m. Diamonds represent locations of CTD casts by NPS (blue) and APL-UW (green, orange, and red).

Figure 5. ICEX Map for 2016 and 2018

C. EQUIPMENT

1. Echosounder

The NPS field team deployed the BioSonics DT-X Extreme scientific echosounder during ICEX-18. The echosounder has a system noise floor of -140 dB, a dynamic range of 160 dB, ping rates ranging from 0.01–30 pings per second, pulse duration ranging from 0.1–1.0 ms, and has six digital transducers with frequencies ranging from 38–1000-kHz (BioSonics 2018). The digital transducer used during ICEX-18 operated at 120-kHz with a SL of 219.8 dB, a beamwidth of 7.9°, a ping rate of 5 pings per second, a pulse duration of 0.5 ms, and a receiver sensitivity of 47.5 dB at a depth of two meters.

2. Acoustic Doppler Current Profiler

NPS employed a 300-kHz Teledyne Marine RDI Workhorse Sentinel ADCP during ICEX-18. The specification sheet provided by Teledyne Marine (2009) states the ACDP has a typical range of 83 meters with a standard deviation of 14 cm s^{-1} when the depth cell size is set to one meter. Additionally, the ADCP profiles a velocity range between ± 5 m s^{-1} and ± 20 m s^{-1} with a velocity accuracy to within 0.5% of the water velocity relative to the ADCP ± 0.5 cm s^{-1} and a velocity resolution of 0.1 cm s^{-1}. Finally, a fluxgate-type compass within the ADCP is accurate to within ± 2° and precise to within ± 0.5° with a resolution of 0.01°.

3. Conductivity, Temperature, and Depth Profiler

The RBR*concerto*^{3} CTD provided the single profile obtained by NPS during ICEX-18 to a depth of approximately 100 meters. The RBR*concerto*^{3} sampled at a rate of 0.5-Hz during the data collection. According to the RBR*concerto*^{3}'s specification sheet provided by RBR (2018), it samples conductivity within a range of 0–85 millisiemens (mS) cm^{-1} with an accuracy of ± 0.003 mS cm^{-1} and a resolution of 0.001 mS cm^{-1}. It also states that temperature is sampled with a range of -5°–35°C with an accuracy of ± 0.002°C and a resolution of 0.00005°C. For this instrument, depth was set at a threshold of 500 meters. The depth is recorded with an accuracy of ± 0.05% full scale and a resolution of 0.001% full scale (RBR 2018).

The Applied Physics Laboratory at the University of Washington (APL-UW) utilized the SeaBird SBE 19 SEACAT Profiler CTD for their profiles during ICEX-18 to an approximate depth of 500 meters. The SBE 19 SEACAT sampled at a rate of 2-Hz during the data collection. According to the user's manual provided by Sea-Bird (2006), it samples conductivity within a range of 0–7 Siemens (S) m^{-1} with an accuracy of ± 0.001 S m^{-1} and a resolution of 0.0001 S m^{-1}. Also, temperature is sampled with a range of -5°–35°C with an accuracy of ± 0.01°C and a resolution of 0.001°C. Finally, the depth is recorded with an accuracy of ± 0.02% full scale and a resolution of 0.001% full scale.

4. Acousonde

The Acousonde 3A Underwater Acoustic Recorder used by the NPS field team during both ICEX-16 and ICEX-18 allows for the recording of acoustic signals as well as the logging of three-dimensional (3D) tilt, 3D compass, temperature, and depth (Acoustimetrics 2013). While the Acousonde 3A recorder performed each of these functions during the ICEX-16 experiment, the only data of interest for this study are obtained from the 3D compass. The Acousonde 3A samples 3D compass measurements at a rate of 40 Hz with a sampling resolution of 16 bits (Acoustimetrics 2013).

IV. DATA ANALYSIS

MATLAB and Visual Acquisition 6.3, the accompanying software for the echosounder, were utilized to perform analysis on the various types of collected data. Data collected from Acousonde recorders, the ADCP, CTDs, and echosounder were analyzed using MATLAB while Visual Acquisition assisted in the analysis of the echosounder data.

A. INITIAL ASSUMPTIONS

In order to conduct data analysis, two, major assumptions were required to be made before the analysis could begin. First, based on calculations with the given digital-transducer source level, the range between the transducer and echogram returns, and the values labeled as EL, along with a confirming phone conversation with BioSonics technical support, the value referred to as EL in their echogram products from Visual Acquisition does not match the accepted definition of EL discussed in Chapter II. Rather, the value referred to as EL matches the traditionally-accepted definition of TS. This value will continue to be labeled EL, but it will be viewed in the same manner as TS for follow on calculations. Additionally, since the NPS CTD cast was the only recorded CTD during the echosounder and ACDP recording, and it only measured to an approximate depth of 100 meters, it will be assumed that the NPS profile matches those of the APL-UW profiles below the 100-meter depth if they were shifted upwards by 15.5 meters as shown in Figure 6. While this is not ideal, and there is no way to definitively know the characteristics of the profile during the data collection below 100 meters, this assumption will allow for further analysis to be conducted and hypothetical conclusions to be drawn. The variability below 100 meters is known to be low, and it is confirmed in the CTD profiles from APL-UW, making this a reasonable assumption.

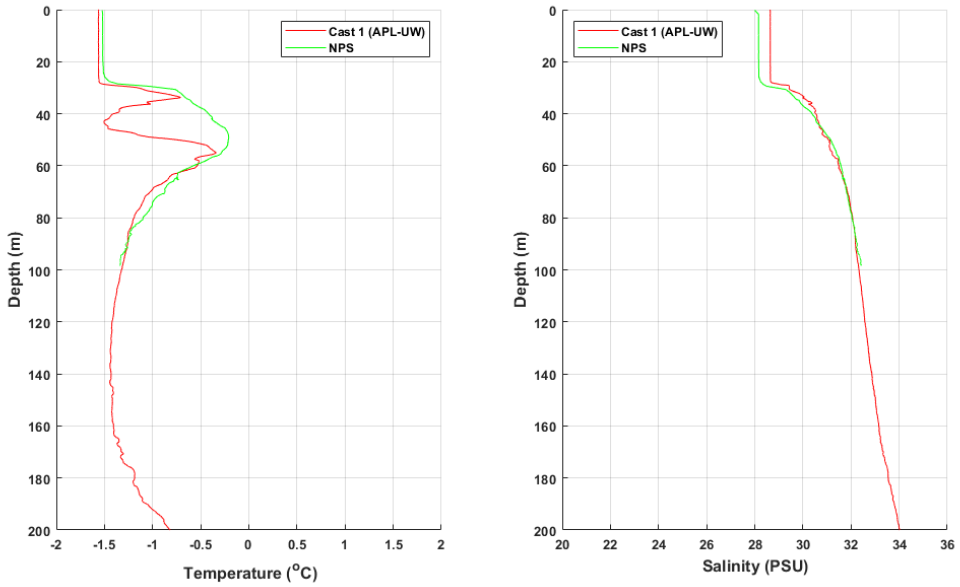

Figure 6. 15.5 Meter Shifted APL-UW Profiles with NPS Profiles

B. VISUAL ACQUISITION

Visual Acquisition 6.3 provides a user interface that allows for the display of echosounder data in various forms. The software allows the user to split or append data files in order to view as little or as much data at one time as the user desires. The data in this study were collected in 30-minute files with the final file being slightly shorter. Upon loading of a data file, the software presents the user with an image similar to what is shown in Figure 7. The initial image presents the full depth of data with an EL amplitude range from 0 to -130 dB and only a selected number of beginning pings in the data file.

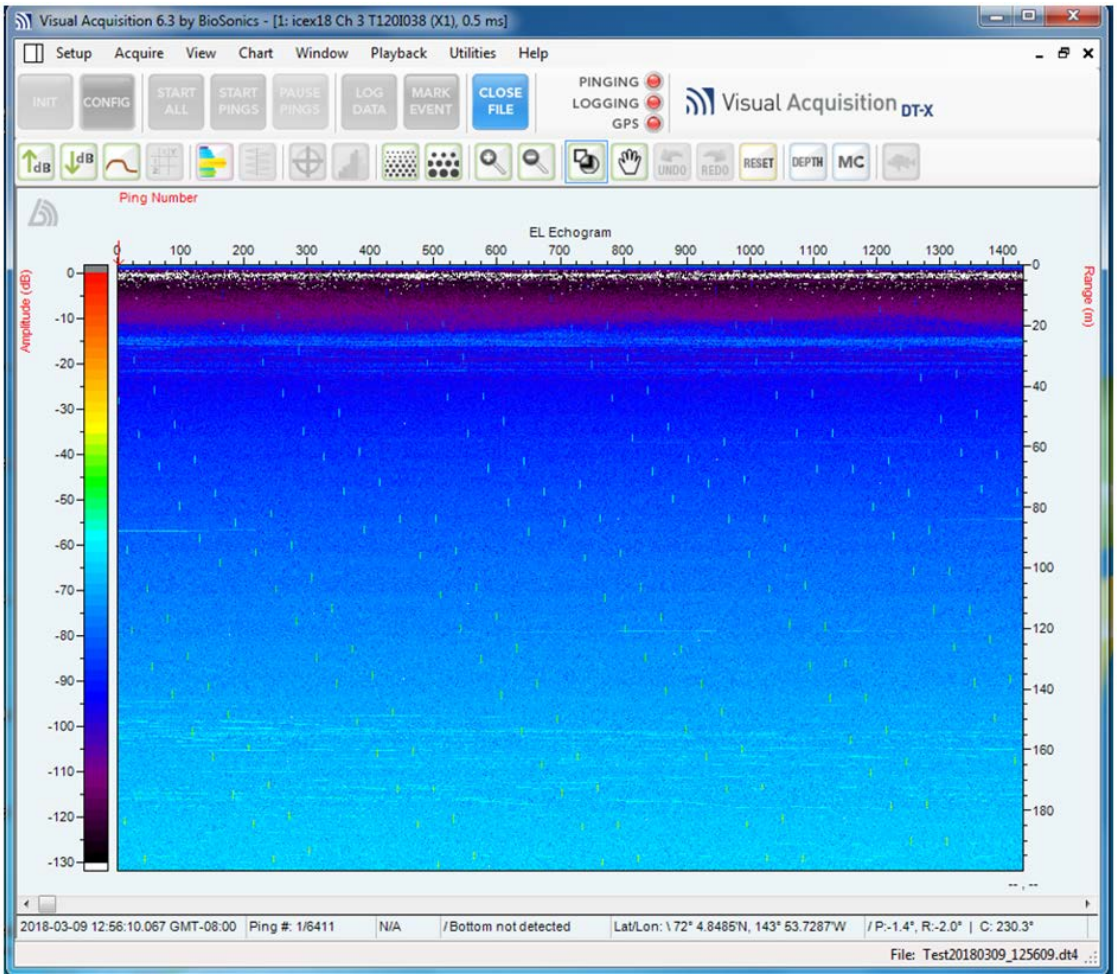

Figure 7. Initial Data Display in Visual Acquisition 6.3 User Interface

In order to present the entire data file, the view was changed from echogram full resolution to echogram overview. Next, to highlight the echo returns within the data, two alterations to the range and color scale of the EL were made. First, the display threshold was decreased from a value of -130 dB to -150 dB. Finally, the color sensitivity was increased to change the upper bound of the color scale from 0 dB to a value of -55 dB. These three modifications to the original display resulted in the graphic shown in Figure 8.

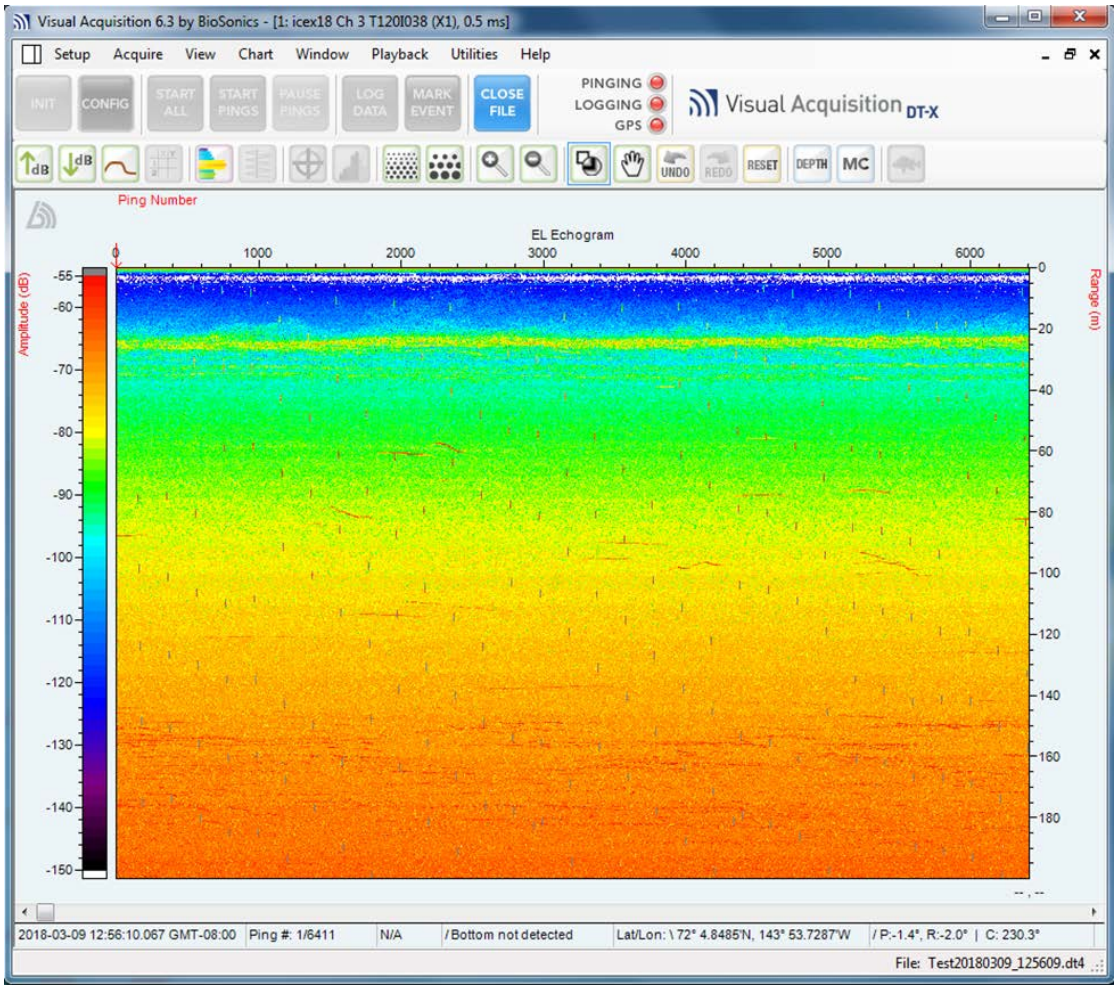

Figure 8. Modified Data Display in Visual Acquisition 6.3 User Interface

Visual Acquisition also allows the user to export various data into comma-separated files and MATLAB MAT-files. Data able to be exported include EL in a 40 log r domain, a 30 log r domain typically used for bottom mapping, volume-scattering strength values in a 20 log r domain, and a raw-counts format measuring the analog to digital converter counts. Once exported into these file types, all further data analysis occurred using MATLAB.

C. MATLAB

1. Echosounder

To begin the analysis of echosounder data in MATLAB, the EL data were loaded into MATLAB from the exported MAT-files. The data were then flipped upside down to place the data closest to the ice at the top of the matrix. Plotting the data using the function pcolor.m produced the image shown in Figure 9. This image confirmed the ability to display the data in a similar manner within MATLAB as Visual Acquisition provides. The next step in analyzing the data consisted of removing false data, artifacts, and background noise from the data in order to more clearly display echo signals with sufficient signal-to-noise ratio to be considered acoustic returns from true ocean features.

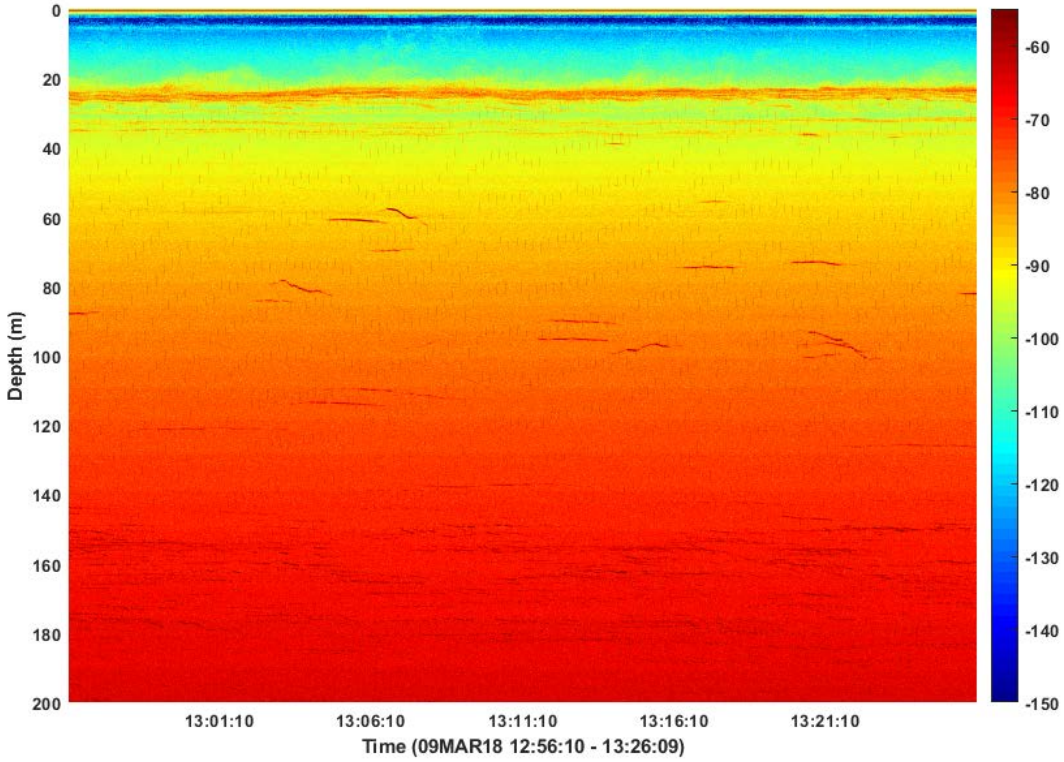

Note: The colorbar on the right represents EL in units of dB.

Figure 9. First 30 Minutes of Original 120-kHz Echosounder Data

From a quick look at the data, it became apparent bad or missing data were labeled with a value of -1000 dB. To remove this from the data, every value less than or equal to -1000 dB was replaced with the Not-a-Number (NaN) placeholder. The NaN placeholder allows for improved plotting of the data without distorting the range of the colorbar or negatively impacting any future calculations conducted on the data. Next, the task of removing the artifact marks dispersed throughout the data as seen in Figures 7, 8, and 9 began. The regular pattern of ticks in the data are believed to be the result of active transmissions from another nearby source at the ice camp that were occurring simultaneously with the NPS echosounder data collection. By zooming in on the image in MATLAB, it became apparent the marks occurred for a width of only one ping. To remove the marks without potentially removing echo returns near them, all data points were compared to the data points one ping before and after them at the same depth they were recorded. If the absolute value of the difference between the current ping and both the ping before and after it was greater than 15 dB, then the NaN placeholder replaced the value within the current ping because it corresponded to an artifact mark. This threshold was utilized because horizontal gradients of that magnitude are not expected in that manner.

Following the removal of artifact marks, the background noise associated with data processing needed to be removed. To accomplish this, the data from two separate pings that both clearly contained echoes throughout the depth record were plotted together using both the EL and raw-counts data sets, as shown in Figure 10 and Figure 11, respectively. In Figure 10, the underlying 40 log r curves that the data fall on are readily apparent, but they alone do not provide a clear line of distinction between background, processing noise and real, echo returns. Only after the raw counts were plotted for the two pings did it become clear where potential cut-off values could be established. For this study, all raw-counts data with a value of greater than or equal to 250 or less than or equal to 10 were replaced with the NaN placeholder. Afterwards, any index within the raw-counts matrix containing NaN had a NaN placeholder inserted into the same index within the EL matrix.

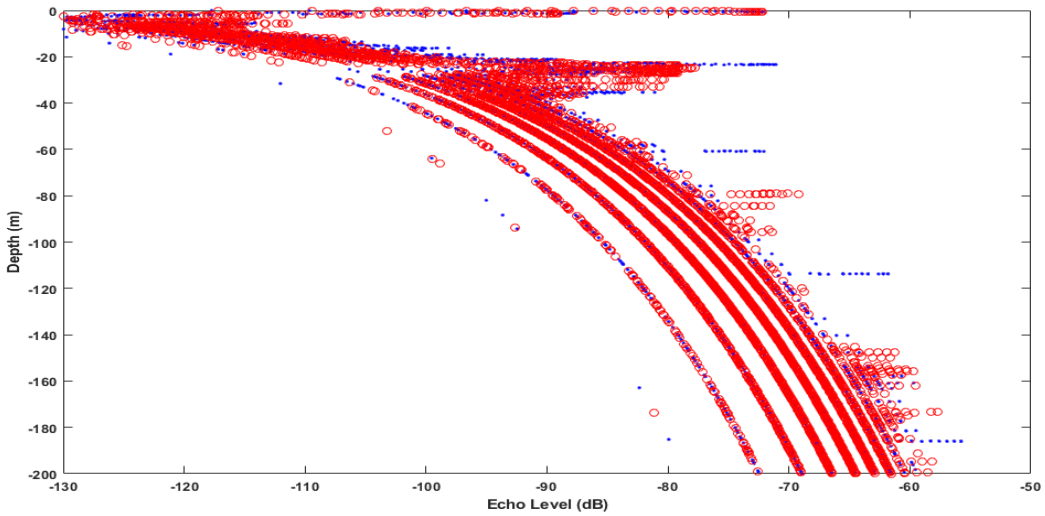

Note: Red circles and blue dots represent the echo level recorded at two single, separate pings for all depths within the data record.

Figure 10. Echo Pings with 40 log r Fit

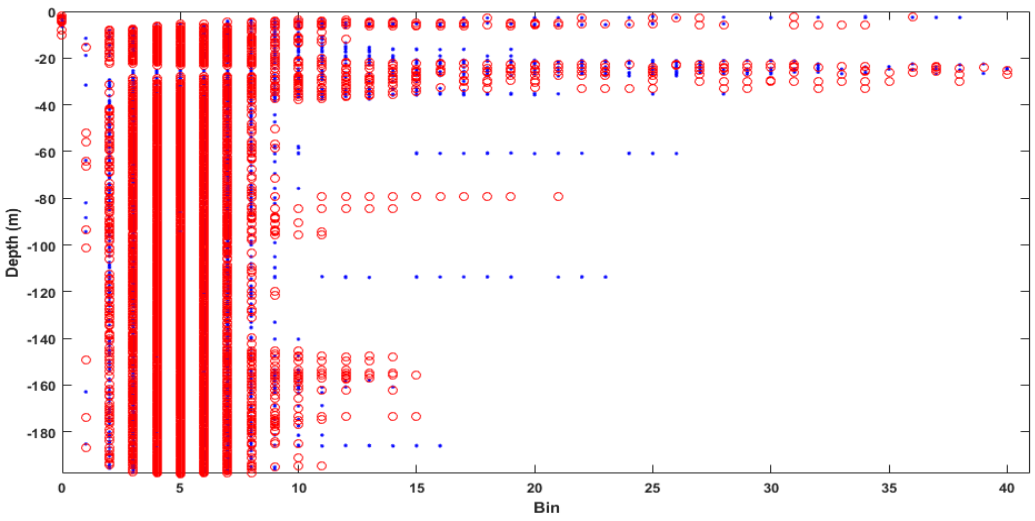

Note: Red circles and blue dots represent the raw counts collected at two single, separate pings for all depths within the data record.

Figure 11. Echo Pings Displayed as Raw Counts

Following the removal of bad data, artifacts, and background, processing noise, the EL data were ready to be displayed in a clear manner. The first 30 minutes of recorded data

are displayed in Figure 12. With those items removed, the location of echo returns becomes much easier to determine. The plots of the remaining data records are contained within Appendix A.

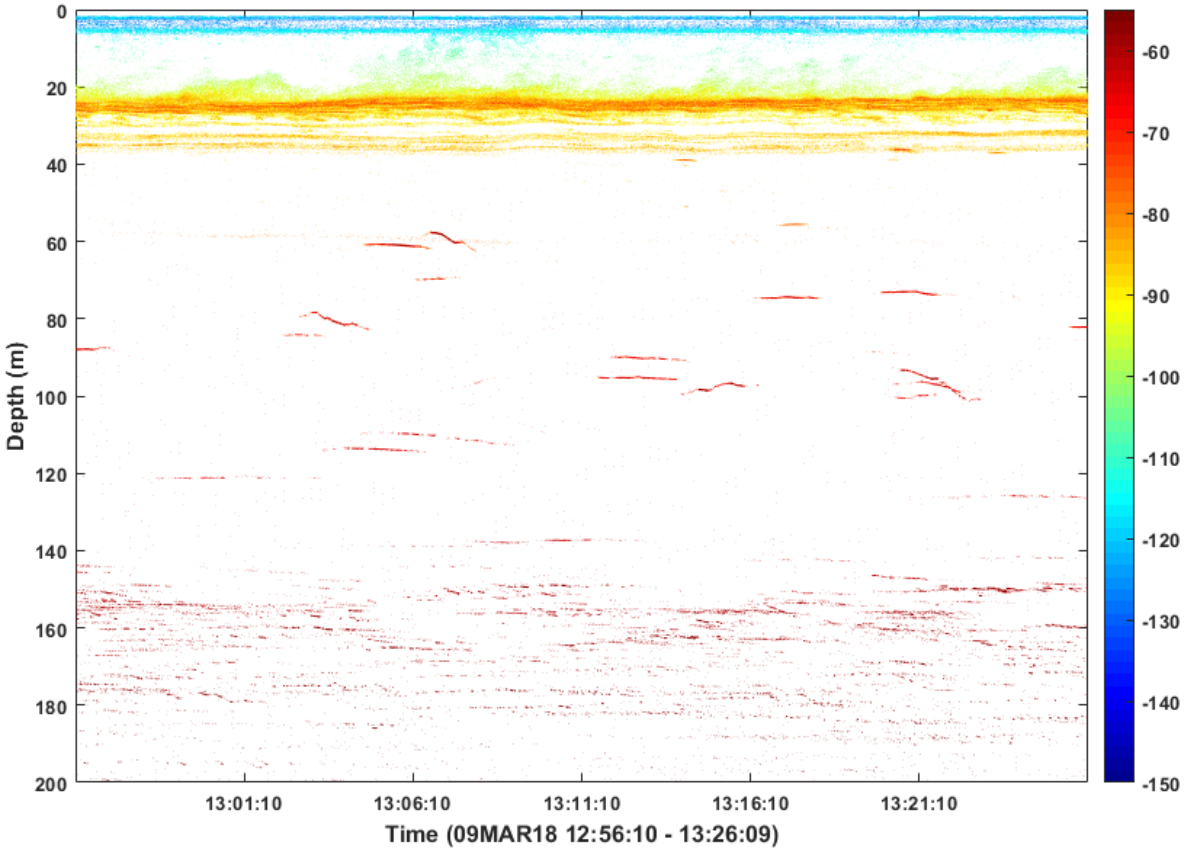

Note: The colorbar on the right represents EL in units of dB.

Figure 12. First 30 Minutes of Noise-Removed 120-kHz Echosounder Data

2. Acoustic Doppler Current Profiler

Analysis of the ADCP data began with loading the available MAT-files and assigning the data to variables. The available data included magnitude and horizontal and vertical velocity components relative to the ADCP in units of mm s^{-1}, and direction relative to the ADCP in units of tenths of a degree. Upon looking at the data, it became evident missing data were indicated by readings of -32768. Each index within the data where this

value occurred were replaced with the NaN placeholder. Each velocity measurement was converted from mm s^{-1} to cm s^{-1}, and each direction measurement converted from tenths of degrees to degrees. The ADCP data were recorded across 30 two-meter-thick depth bins, so velocity was averaged across each depth bin. The average horizontal-velocity components, u and v, for each depth were used to calculate the average relative direction at each depth using the equation

$$\theta = \tan^{-1}(v / u). \tag{6}$$

The relative directions were adjusted to match the appropriate quadrant for the given u and v components. Following this calculation, the magnetic, relative directions were converted to true, relative directions by adding a declination of 19.669 °E calculated based on the location and date of the ADCP measurements using a magnetic-field calculator provided by the Government of Canada (2018). Next, the true, relative directions were converted back to true horizontal-velocity components using the equations

$$u = r \cos\theta \tag{7}$$

$$v = r \sin\theta, \tag{8}$$

where r is the magnitude of the water velocity relative to the ADCP. The next step consisted of calculating the distance traveled by the ice during the recording of data. The latitude and longitude of the starting and ending points of collection were used with the MATLAB distance function from the mapping toolbox. The distance function provided the total, ice travel in units of degrees of longitude. The distance was converted first to kilometers and then to nautical miles. The distance in nautical miles was divided by the total time of collection to determine velocity of the ice in knots. The velocity was then converted from knots to cm s^{-1}. The direction of ice travel was calculated via a calculator provided by Movable Type (2018). The velocity and direction of ice travel were converted to horizontal-velocity components using equations 8 and 9. Next, the horizontal-velocity components of the ice motion were subtracted from the horizontal-velocity components of the ADCP measurements to produce the true horizontal-velocity components of the water.

These horizontal-velocity components were converted to a true magnitude using the equation

$$r = \sqrt{u^2 + v^2} \ . \tag{9}$$

Both the true magnitude and horizontal-velocity components were then averaged across each of the depth bins. Finally, the averaged horizontal-velocity components were converted to average, velocity directions using equation 7. With this set of calculations complete, the graphs displayed in Figure 13 were produced, representing velocity components, horizontal-velocity magnitude, and velocity direction in both relative and true. The top row is measured relative to the ADCP, and the bottom row is the true measurement with the motion of the ice subtracted from the recorded data. It is shown in (e) and (f) that the horizontal velocity and direction are coupled to the ice, but this coupling weakens quickly with depth.

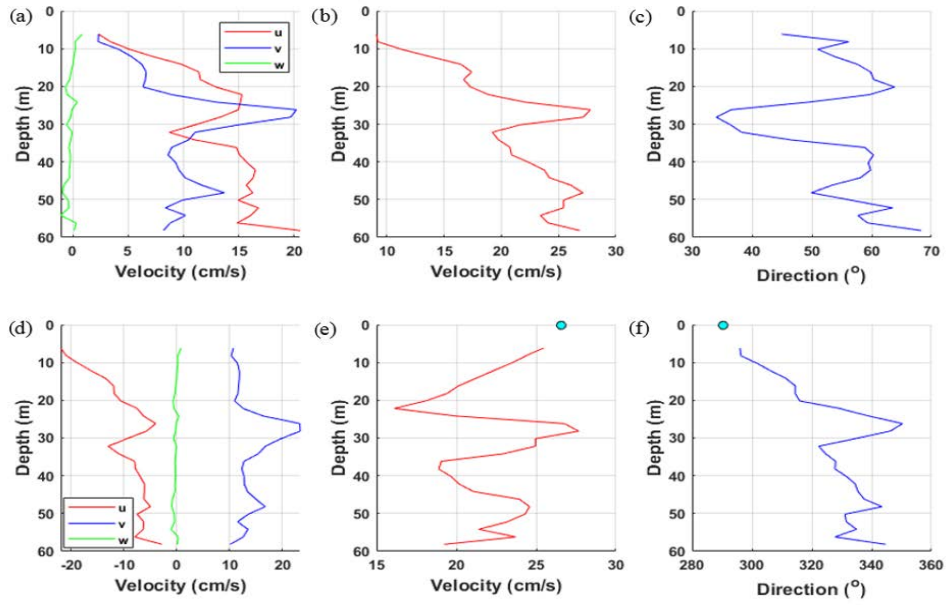

From top left to bottom right, top row first. (a) u, v, and w component velocities relative to the ice. (b) Velocity magnitude relative to the ice. (c) Velocity direction relative to the ice. (d) u, v, and w component true velocities. (e) True, horizontal-velocity magnitude of the water. Teal dot indicates velocity of the ice motion. (f) True velocity direction of the water. Teal dot indicates direction of the ice motion.

Figure 13. ADCP Results from ICEX-18

3. Conductivity, Temperature, and Depth Profiler

Of the two CTDs deployed by the NPS team, only the one at 100 meters is included in this data analysis because the CTD at 40 meters failed to record data during the experiment. The data from each of the four casts were loaded into MATLAB using the function dlmread.m. The properties for each cast were then defined as variables associated with each cast. The entire record of the APL-UW casts were stored while only the data associated with the upcast were stored for NPS. Next, density was calculated for each of the APL-UW casts utilizing the gsw_rho.m function from the Gibbs-SeaWater (GSW) toolbox (McDougall and Barker 2011). The sound speeds for each cast were plotted on a set of subplots, as seen in Figure 14. Then plots of temperature, salinity, sound speed, and density from each of the four casts were created, as seen in Figure 15. Additionally, plots from APL-UW were shifted up vertically to determine the best assumption for the NPS profile below a depth of 100 meters, as previously discussed in Section A of this chapter.

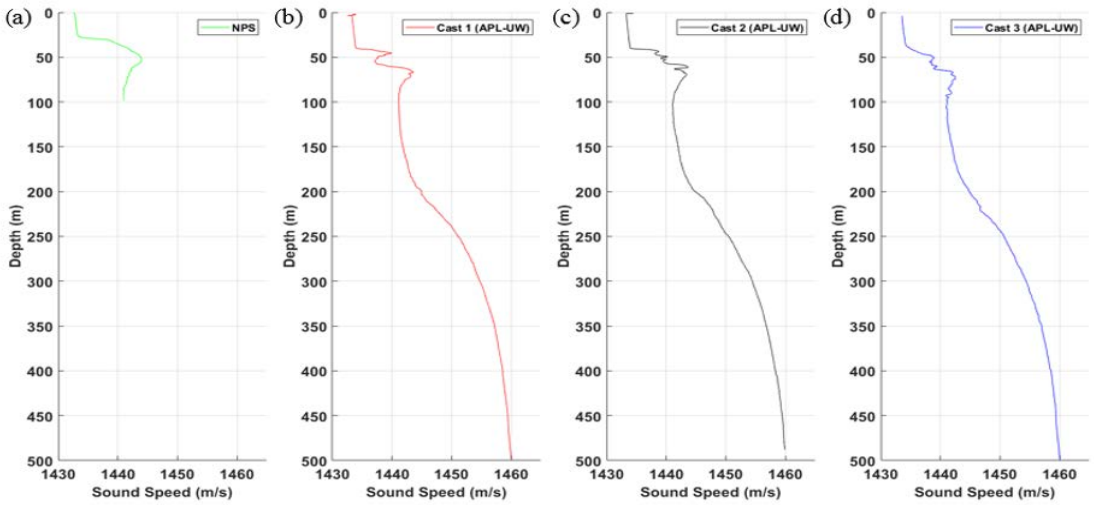

From left to right: (a) NPS profile recorded on 09 March. (b) APL-UW profile recorded on 13 March. (c) APL-UW profile recorded on 14 March. (d) APL-UW profile recorded on 19 March.

Figure 14. Sound Speed Profiles from ICEX-18

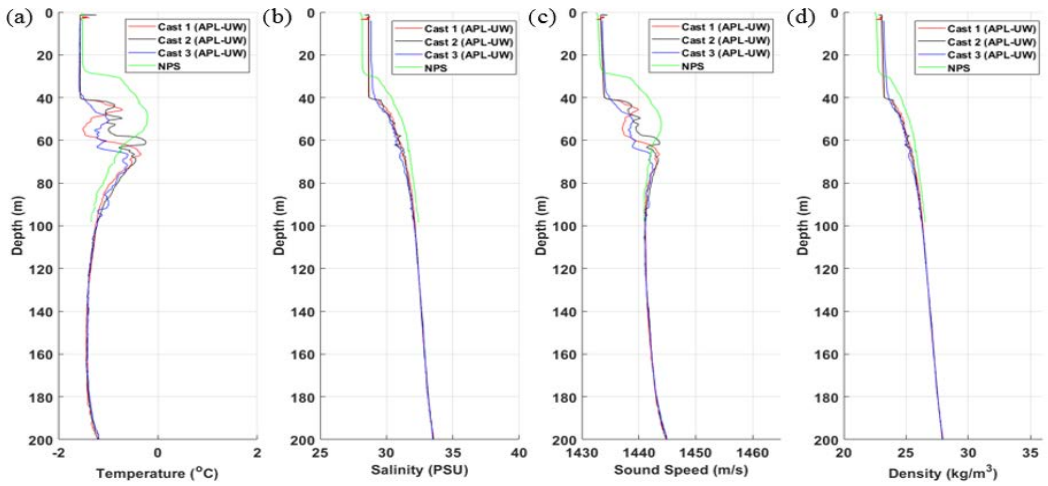

From left to right: (a) Temperature profiles recorded during ICEX-18. (b) Salinity profiles recorded during ICEX-18. (c) Sound speed profiles recorded during ICEX-18. (d) Density profiles recorded during ICEX-18. Note: Each set of profiles contain noticeable variability above 100 meters, but each converges to minimal variability below 100 meters.

Figure 15. Profiles from NPS and APL-UW CTD Casts from ICEX-18

Next, the NPS CTD cast data were used to calculate the reflection coefficient as described by Stranne et al. (2017). First, acoustic impedance is calculated using the equation

$$\eta(z) = V(z)\rho(z), \tag{10}$$

where V is sound speed and ρ is seawater density. Next, the impedance is used to calculate the reflection coefficient using the equation

$$R_{CTD}(i) = \frac{\eta(i) - \eta(i-1)}{\eta(i) + \eta(i-1)}, \tag{11}$$

where each element i has a corresponding depth z(i), and the depth of $R_{CTD}(i)$ is the average of z(i-1) and z(i). The reflection coefficient was then plotted versus depth for the NPS CTD cast as shown in Figure 16.

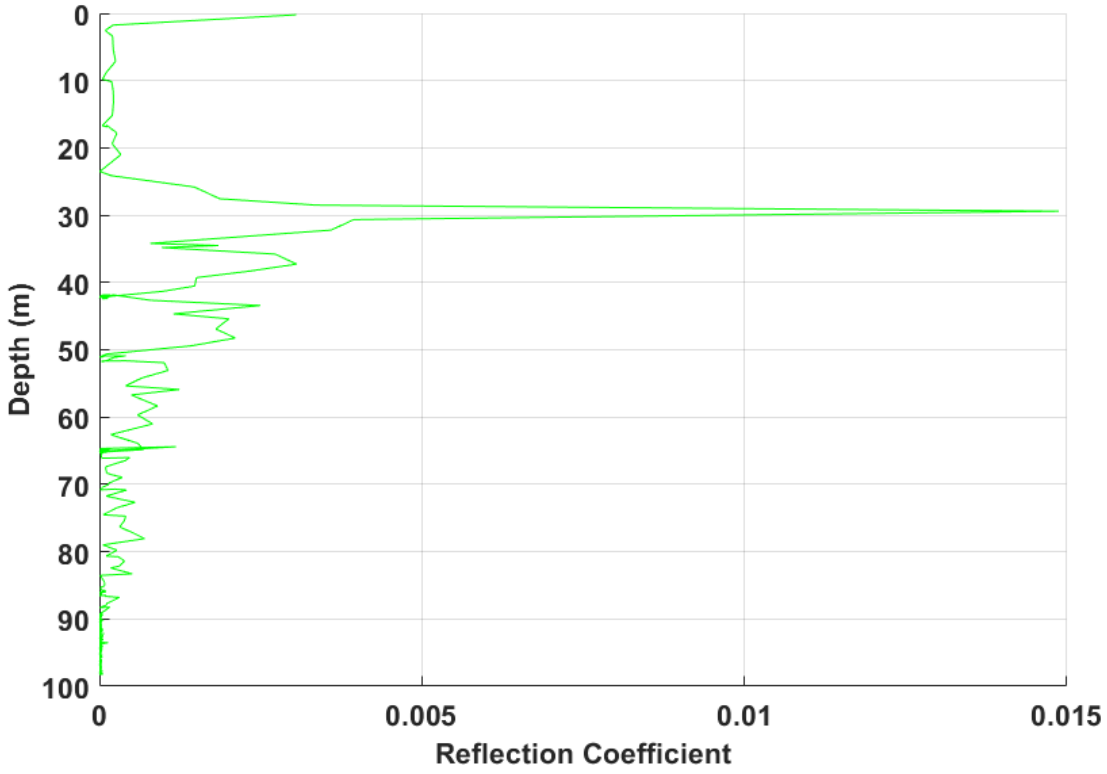

Note: The CTD cast used to calculate the reflection coefficient did not occur at the same time as the echosounder data collection.

Figure 16. Reflection Coefficient for NPS CTD Cast

4. Acousonde

Only Acousonde recorder data from ICEX-16 were used during this analysis. The data collected during ICEX-18 were contaminated with noise from helicopter operations conducted approximately 10–20 meters from the location of the experiment. The auxiliary data, to include temperature, pressure, time, compass components, and accelerometer components from the Acousonde recorder used during the short-range acoustic propagation described in Nelson (2016) were loaded into MATLAB and stored into variables. The accelerometer data were recorded in units of milligravitation (earth). They were converted to cm s^{-2} by multiplying by 0.981. The running standard deviations of the X, Y, and Z accelerometer components of the recorder were calculated over a range of 20 data points

during the upcast of the recorder. This created a vertical profile of each component's standard deviation, and it is shown in Figure 17.

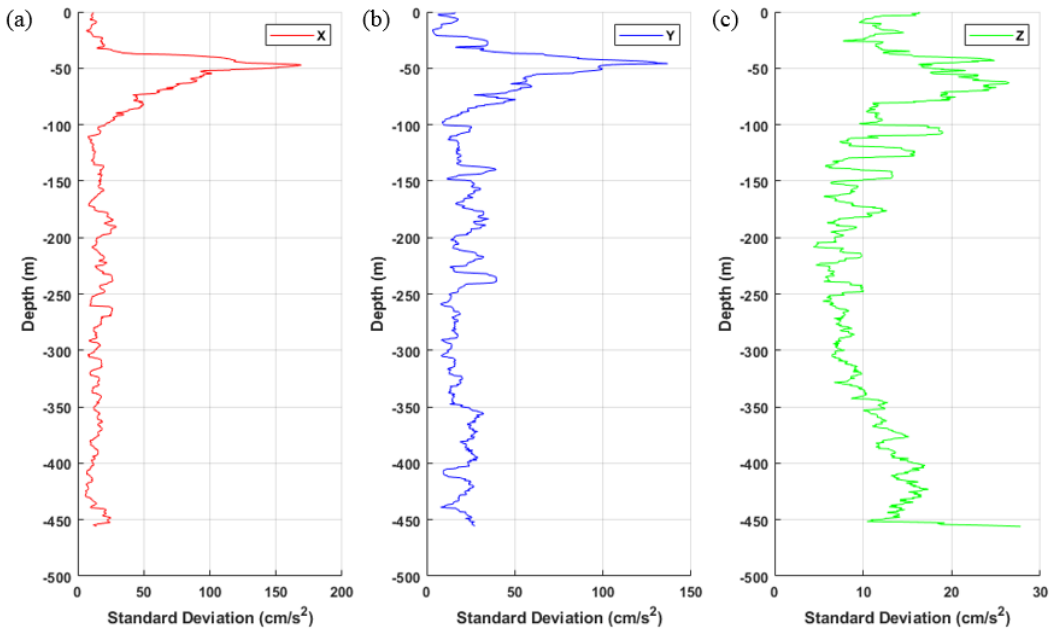

From left to right: (a) Along-axis accelerometer standard deviation (b) Across-axis accelerometer standard deviation. (c) Down-axis accelerometer standard deviation. Note: Each direction experiences a maximum in standard deviation near 50 meters, the depth of the thermocline during ICEX-16.

Figure 17. Acousonde Accelerometer Standard Deviation from ICEX-16

V. DISCUSSION

A. RESULTS

Upon completion of the data analysis, further elaboration on the findings and their oceanographic significance is in order. The three observations meriting discussion are the fine structure detected in the echosounder data, the turbulence recorded from the echosounder, ADCP, and Acousonde recorder, and the acoustic variability documented in the CTD data.

1. Fine Structure

The echo returns from the echosounder present an elaborate field of fine structure throughout the water column beneath the ice. When viewed next to the temperature and salinity profiles coinciding with the time of data collection, as in Figure 18, the seemingly random array of returns begins to present a clearer picture of their arrangement. One of the most noticeable features within the echosounder data is the solid line of returns of approximately -65 dB at a depth of 25 meters. From the profiles of temperature and salinity, it is seen that those returns correspond to the thermocline and halocline of the PSW present at the base of the surface mixed layer.

Below the PSL, intermittent regions of little to no returns occur between a region of sparse returns and a deeper region where the returns begin to stack in a layering manner. At a depth of approximately 50 meters, a region of little to no returns is seen in the echosounder data. This happens to coincide with the NSTM where the temperature gradient is zero. In the region below the NSTM in the NPS profile, from approximately 60 to 120 meters, there are widely dispersed returns throughout the water column. Within this same depth range, the temperature gradient becomes negative. A negative temperature gradient is not conducive to the formation of thermohaline staircases, however, this gradient is indicative of a salt finger regime (Bebieva and Timmermans 2017). Therefore, these returns are possibly caused by thermohaline intrusions, similar to those discussed in Bebieva and Timmermans (2017), only these are occurring above the staircase regime instead of below it. The echosounder returns are a result of strong, vertical-sound-speed gradients that may occur along isopycnals. The intrusions may only create these strong gradients in certain locations so the returns tend to be

randomly distributed at different depths. Between approximately 120 and 140 meters, another region with little to no returns exists. This region also contains a temperature minimum, where the gradient becomes zero. Below 140 meters, the returns become elongated and form in a layer-like fashion separated vertically by a few meters, similar to diffusive staircases observed by ITPs and Stranne et al. (2017). In both the temperature and salinity profiles, a significant change occurs at 140 meters. In the temperature profile, the gradient turns positive and begins to strengthen with depth. In the salinity profile, there exists an inflection point at 140 meters where the gradient starts to increase positively with depth at a higher rate. While the temperature and salinity gradients are not large enough to produce thermohaline staircases as seen in Stranne et al. (2017), the formation of returns in this manner below 140 meters indicate the likely existence of staircases at greater depths. In Stranne et al. (2017), they were about to take CTD casts simultaneously during the collection of echosounder data, allowing them to calculate the reflection coefficient and correspond the peaks in reflection coefficient with the existence of temperature and salinity gradients and thermohaline staircase returns in the echosounder. Because the NPS CTD data were collected after the retrieval of the echosounder, we are unable to compare Figure 16 directly with any echosounder data. We hope to accomplish this in ICEX-20.

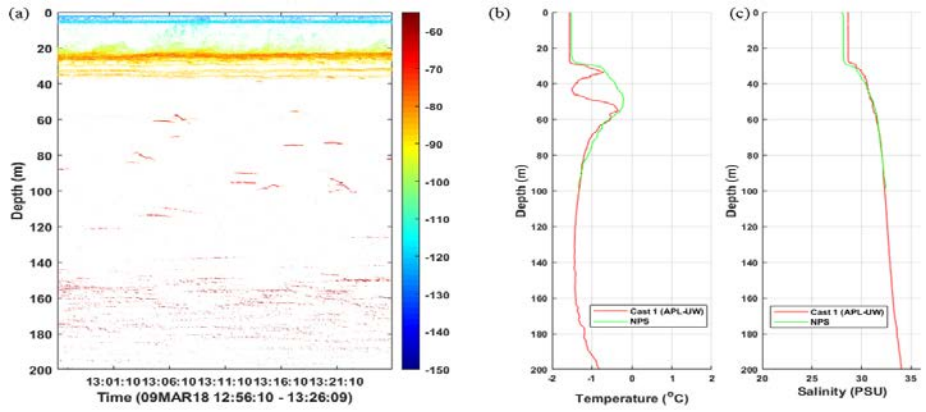

From left to right: (a) Echosounder data with noise removed, representative of the entire data set. Note: The colorbar on the right represents EL in units of dB. (b) Temperature profiles from NPS and APL-UW. (c) Salinity profiles from NPS and APL-UW. Both APL-UW profiles are shifted up 15.5 meters.

Figure 18. Comparison of Echosounder and CTD Data from ICEX-18

While it would be more scientifically significant if the returns were, in fact, caused by fine structure, it is not the only possible source of high reflectively in the water. Another possibility for the cause of the echosounder returns is biological detection, whether it be fish or plankton. To demonstrate the EL returns measured below 50 meters in the experiment differ from that expected by biological organisms, the expected TS of a wide range of fish sizes with the frequency used in the experiment were calculated. TS of a fish at dorsal aspect is given by the following empirical equation:

$$TS = 19.1 \log_{10} L - 0.9 \log_{10} f - 54.3, \tag{12}$$

where L is the fish length in inches and f is the frequency of the source in kilohertz (Urick 1983). Using this equation and the 120-kHz frequency of the echosounder, TS for various lengths of fish were plotted, as shown in Figure 19. Given the upper threshold of -55 dB, plotted as the dashed-red line in Figure 19, and considering most of the returns in the data occur at -65 dB, then those fish providing returns would be at lengths of on the order of one-half inch or shorter.

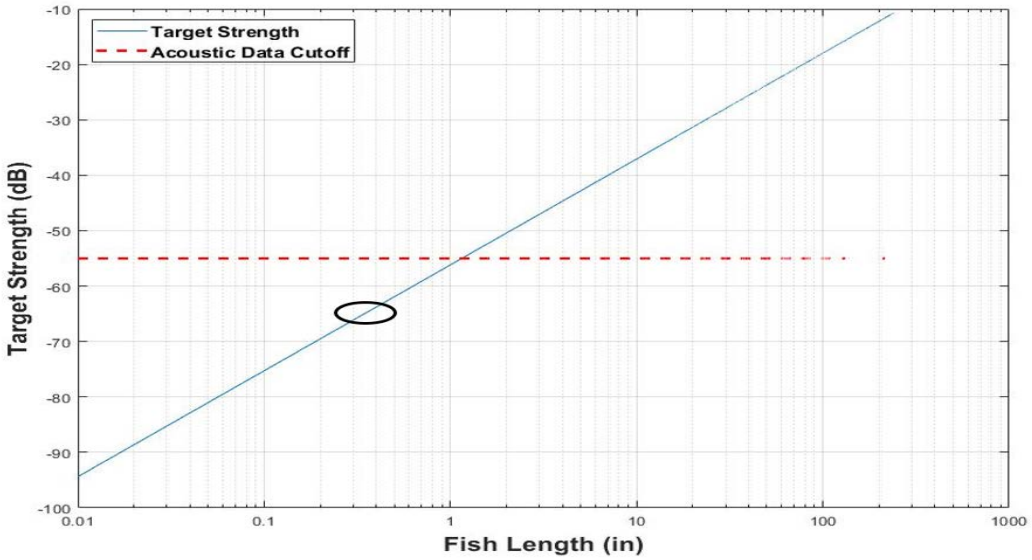

Note: The black oval represents the EL of the returns in the echosounder data. In order for a fish to produce those returns, it would at lengths of on the order of one-half inch or shorter.

Figure 19. Target Strength vs. Fish Length at 120-kHz

In order to show the necessary conditions under which biological organisms could cause the returns found below the PSL, multiple sources were consulted to determine the typical TS values for fish and plankton found in the Arctic Ocean. Based on McBride et al. (2014), the dominant species of organisms inhabiting the Arctic Ocean are capelin, cod, euphausiids, and copepods. Then, using Simmonds and MacLennan (2005) it was calculated using the equation

$$TS = 20 \log L + b_{20}, \tag{13}$$

where L is the length in cm and b_{20} is a parameter derived from linear regression in dB, that a cod must be 1.12 cm long and a capelin must be 1.03 cm long to produce returns of -65 dB at a frequency of 120 kHz. Fish that small in size seem unlikely to be the producers of the returns in the echosounder data, given the fact that the returns are spread out and not concentrated like a school of fish (BioSonics 2017). For a 10 mm euphausiid and a 1 mm copepod, Holliday and Pieper (1980) show that maximum TS of these species never exceeds -100 dB. Many of these organisms combined to form a scattering layer would only raise this value to approximately -90 dB, still well below the returns found on the echosounder. Therefore, it is unlikely that the cause of returns below the PSL in the echosounder data were caused by biological organisms.

2. Turbulence and Shear

Data collected from the echosounder, ADCP, and Acousonde recorder provide evidence of turbulence occurring at or near the interface between the surface mixed layer and the underlying Pacific water. This is demonstrated first in the echosounder data by observing the light-green approximately -100 dB returns billowing upwards from approximately 20 meters depth, just above the consistent return from the PSL, suggesting the presence of shear just below. Also of note in the echosounder data is the apparent tilting to the right of the light-green approximately -100 dB returns between the PSL and ice cover. Looking next at the ADCP data in Figure 13, it becomes clearer that turbulence occurs as a result of velocity and directional shear in the vertical profiles centered on 25 meters. Additionally, it is evident from Figure 13 (e) and (f) that the horizontal velocity and direction of the water directly underneath the ice is coupled to the motion of the ice,

with diminishing velocity and clockwise-directional change down to the PSL at 25 meters, consistent with the findings of Cole et al. (2014). This provides an answer to the cause of the tilting of the light-green approximately -100 dB returns in the echosounder data. Finally, the accelerometer data recorded by the Acousonde during ICEX-16 also showed evidence of turbulence occurring at a depth of 50 meters, corresponding to the level of the PSL at that time. The significant spike in the standard deviation of horizontal acceleration of the Acousonde during ICEX-16 is shown in Figure 17.

3. Acoustic Variability

From an examination of the map in Figure 5 and the sound speed profiles recorded in Figure 14, it is apparent that a considerable amount of variability is present within the Beaufort Sea on spatial and temporal scales of 100s of kilometers and days, respectively. The most striking sign of variability occurs between the NPS profile and the remainder of the profiles recorded by APL-UW. These profiles were recorded on temporal scales ranging from one to five days and spatial scales ranging from approximately 13 to 88 km. The noticeable shallowing of the sound speed gradient in the NPS profile could be the result of a shallower water column due to closer proximity to the continental shelf, or the change in circulation that occurs between the clockwise circulation of the Beaufort Gyre and the eastward flowing Alaskan Coastal Current (Talley et al. 2011). Regardless of the cause, the resulting impact on the acoustic environment is significant. Additionally, the two APL-UW CTD casts from March 13, 2018 and March 14, 2018, displayed in Figure 14 (b) and (c), demonstrate noticeable variability below the main sound speed gradient at depths ranging from 50 to 70 meters. While not as strong as the one found in ICEX-16, the formation of a sound channel below the NSTM, termed the Beaufort Lens, is found in the ICEX-18 data. With more significant peak temperatures in the PSW, as in 2016, the Beaufort Lens becomes stronger and impacts acoustic performance within the sound channel (Baggeroer et al. 2016). This type of variability that is not captured by climatological databases can significantly impact the performance of sonar systems, especially when TDAs are not routinely updated with current environmental data.

B. CONCLUSIONS

1. Oceanographic Significance

These observations are significant to the oceanography of the Arctic Ocean, and they are in keeping with much of the recent literature. Based on the values of the echo returns in the echosounder data, it is likely the returns are caused by the interleaving of water masses, which results in sharp changes to the temperature and salinity gradients. The combination of the shallowing of the PSL, the turbulence associated with the PSL, the pattern of returns corresponding to variations in the temperature and salinity gradients, and the indication the beginning of the thermohaline staircase region might be shallower are critical to the future of the Arctic environment. Timmermans and Jayne (2016) predicted a situation on the verge of formulation based upon the data from ICEX-18, in which reversals of the salinity gradient within the halocline will allow for greater vertical heat transport. The data from ICEX-18 suggest a mechanism for turbulent mixing that will increase the transfer of heat to the surface, further causing the melting of ice. This will have a profound impact on the oceanography and climate of the Arctic Ocean. According to Meneghello et al. (2018), the continued warming of Arctic water could eventually increase the speed and depth of the Beaufort Gyre, having a significant impact on the distribution of freshwater throughout the Arctic Ocean. Continued monitoring and research of the Arctic water column and mechanisms of heat transport will be crucial in accurately predicting the future of sea ice, and ultimately climate, in the Arctic Ocean.

2. Operational Relevance

While the observations of this research are important to the oceanographic community, there more importantly exists an operational relevance to the U.S. Navy in our pursuit to maintain dominance in the undersea domain. The detection and tracking of foreign submarines continues to present challenges to U.S. forces, even in waters with much less complex acoustic environments than the Arctic Ocean. As operations by both submarines and surface vessels become more of a reality within the Arctic Ocean, a vital requirement for protection of our assets will be TDAs that are able to accurately account for the variability in the Arctic Ocean. In environments such as the Arctic, with acoustic

properties changing on the spatial and temporal scales found in this study, it will no longer be acceptable to rely on a single Expendable Bathythermograph (XBT) to determine a range of the day for detection range calculations. In many instances, casting an XBT every hour will not be sufficient to accurately capture the variability of the Arctic environment. Development of systems capable of incorporating continuous, real-time data into TDAs will provide an advantage over any adversaries because of the exploitation of the environment. An additional tactical consideration regarding the environmental variability focuses around the previously mentioned Beaufort Lens. The strength of the Beaufort Lens, controlled by the peak temperature within the PSW, will impact acoustic performance in terms of detection and counter-detection ranges when vessels are operating within the sound speed channel. A stronger sound speed channel will trap more acoustic energy and decrease scattering losses resulting from interaction with the sea ice.

Another operationally-relevant implication drawn from this data consists of the potential deployment of echosounders or newly developed sensors capable of monitoring the status of thermohaline staircases through calculation of the reflection coefficient throughout the water column. This capability, if proven viable through future research, can provide our forces with another method of submarine detection and narrowing of farthest-on-circles, the range of possible locations of a submarine based on its speed and last known location. Developing the capability of deploying this sensor on a multitude of platforms, to include UUVs, ITPs, and the sea floor, with the capacity for network communication amongst other sensors would allow for the creation of a grid to detect submarines. This network would provide optimal performance in locations near entrances to the Arctic Ocean, acting as a tripwire for when the submarine is entering or exiting the area.

3. Future Work

Looking forward to the opportunity for further data collection during ICEX-20, the recommended experiment set-up consists of an echosounder, ADCP, and Modular Acoustic Velocity Sensor (MAVS) continuously recording data for a minimum 24-hour period, and preferably longer if possible, to capture the potential migration of the PSL between day and night, the changes due to various water mass structures at different

locations, and to measure the horizontal velocity shear and turbulence associated with the interaction of the mixed layer and the PSW. Also, lowering an echosounder digital transducer into the water column to conduct a horizontal survey of the water column from various depths would provide a different view of the interleaving occurring throughout the water column, potentially providing further insight to their characteristics and role in the formation of thermohaline staircases. In addition to changing the orientation of the digital transducer, broadcasting at different frequencies will provide greater spectral information, allowing for greater ranges to be surveyed at lower frequencies and higher resolution to be achieved at higher frequencies. Finally, to take the next step in researching thermohaline staircase disruption and subsequent regeneration as a potential source of submarine detection, coordinating the passage of a submarine or similar-shaped submerged object through the field of detection of the echosounder would allow for the in-situ analysis of thermohaline staircase disruption and regeneration patterns and time frames. Conducting many CTD casts while collecting echosounder data, especially during and after the disruption by the submerged object, will allow for the calculation of the reflection coefficient to determine its validity as a potential indicator of thermohaline staircase disruption. In addition to these field experiment suggestions for ICEX-20, further effort should be focused on high-resolution numerical modeling of the fine-scale processes occurring in the Arctic. Modeling can help our understanding of how these fine-scale processes are shaping the structure of the new Arctic.

APPENDIX. NOISE-REMOVED ECHOSOUNDER FIGURES

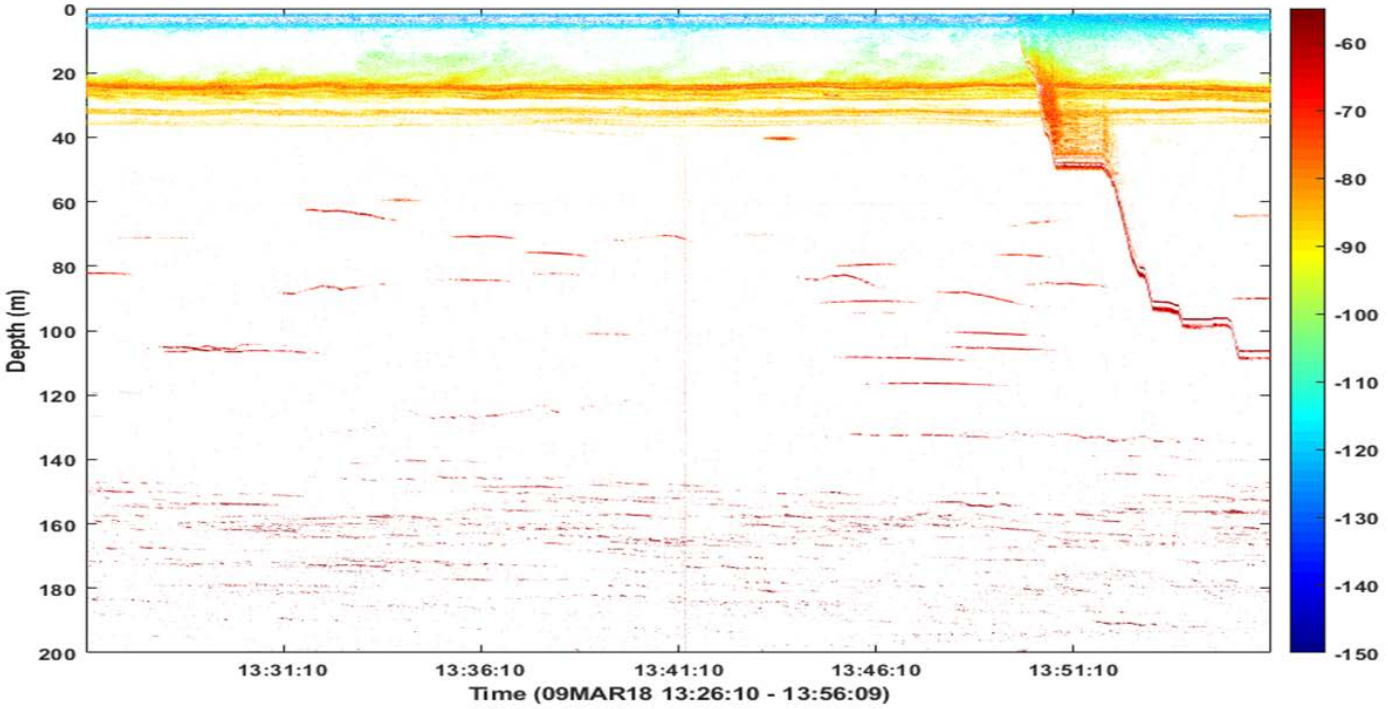

Note: The colorbar on the right represents EL in units of dB.

Figure 20. Second 30 Minutes of Noise-Removed 120-kHz Echosounder Data

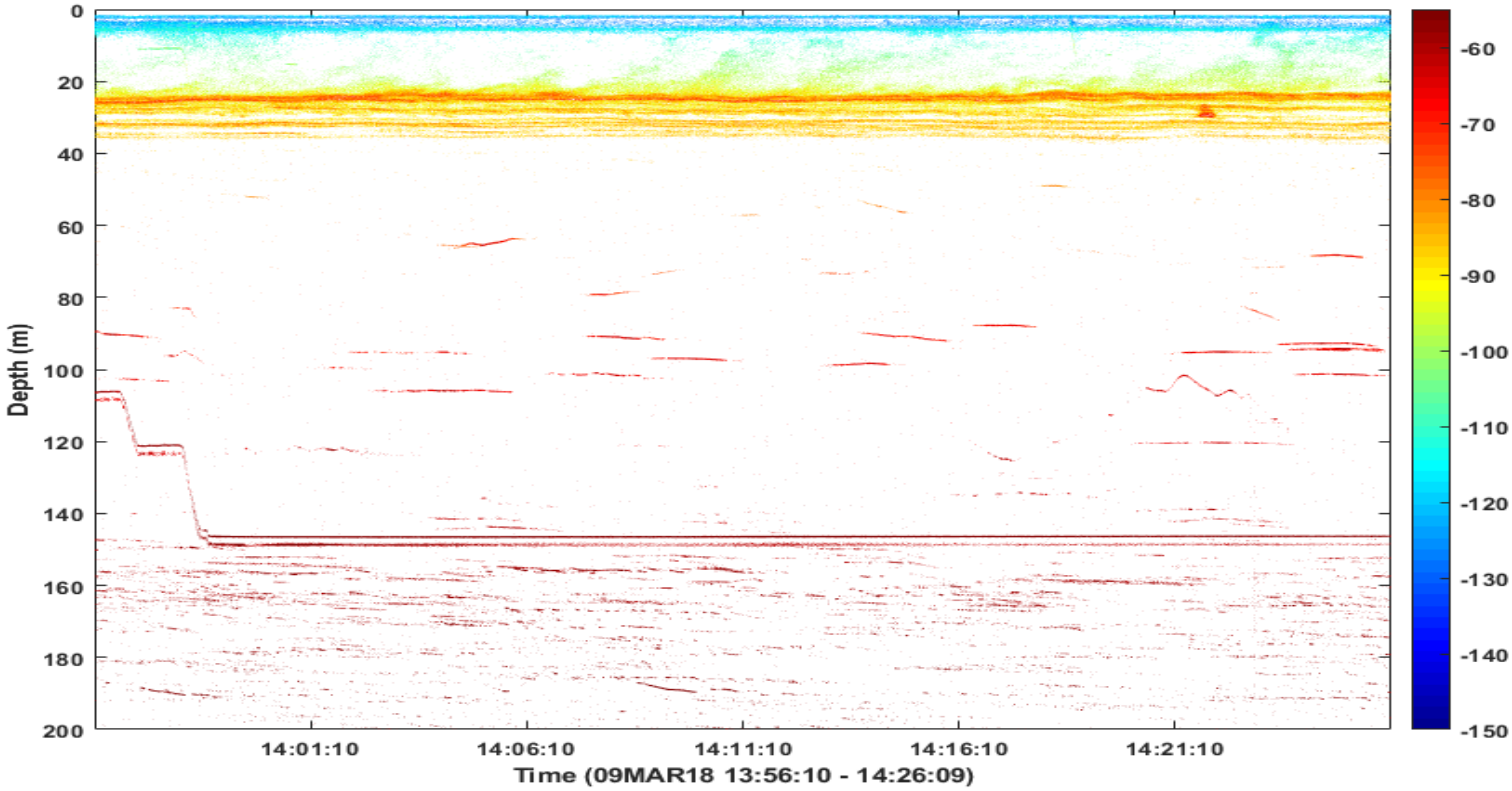

Note: The colorbar on the right represents EL in units of dB.

Figure 21. Third 30 Minutes of Noise-Removed 120-kHz Echosounder Data

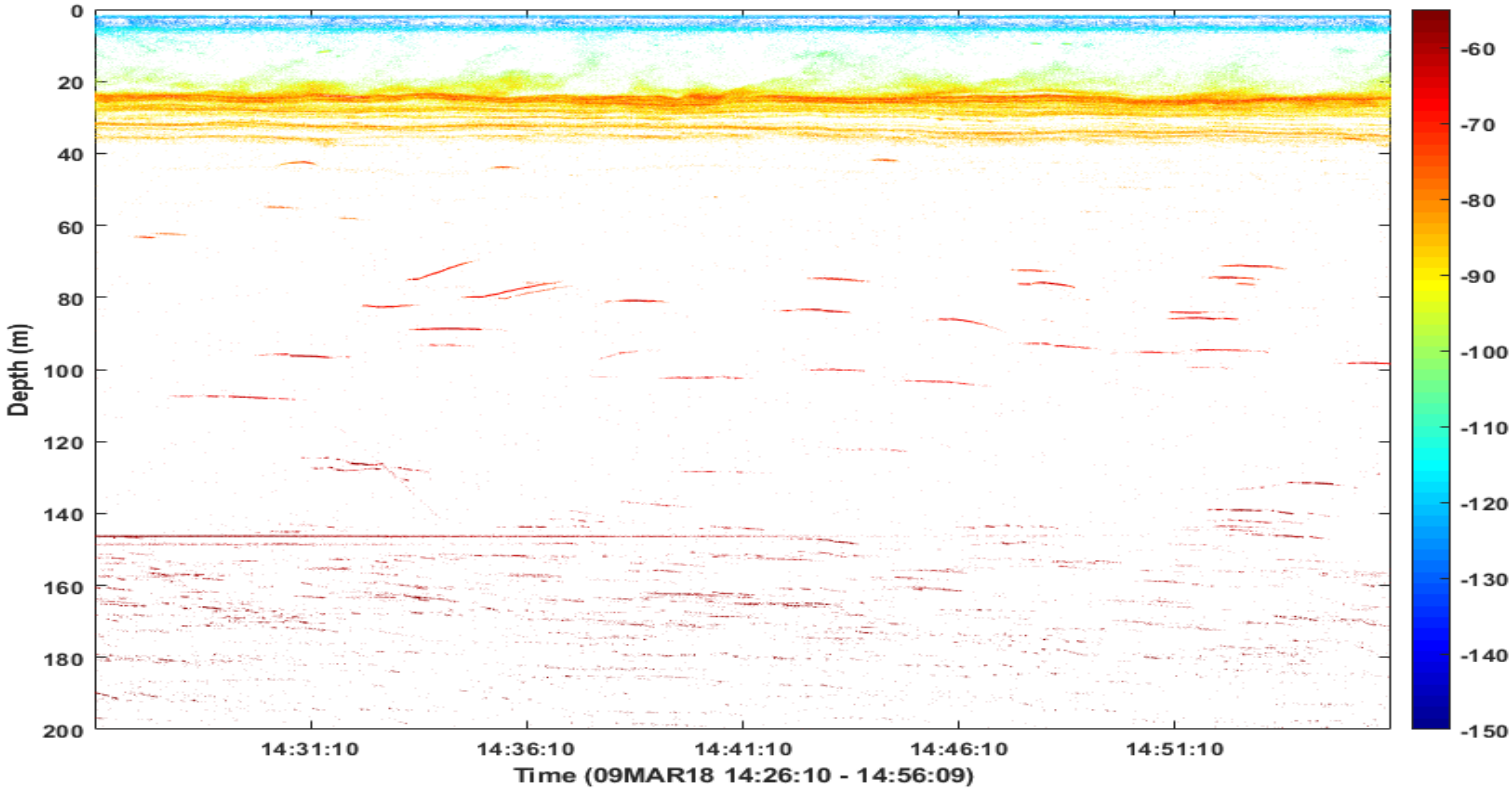

Note: The colorbar on the right represents EL in units of dB.

Figure 22. Fourth 30 Minutes of Noise-Removed 120-kHz Echosounder Data

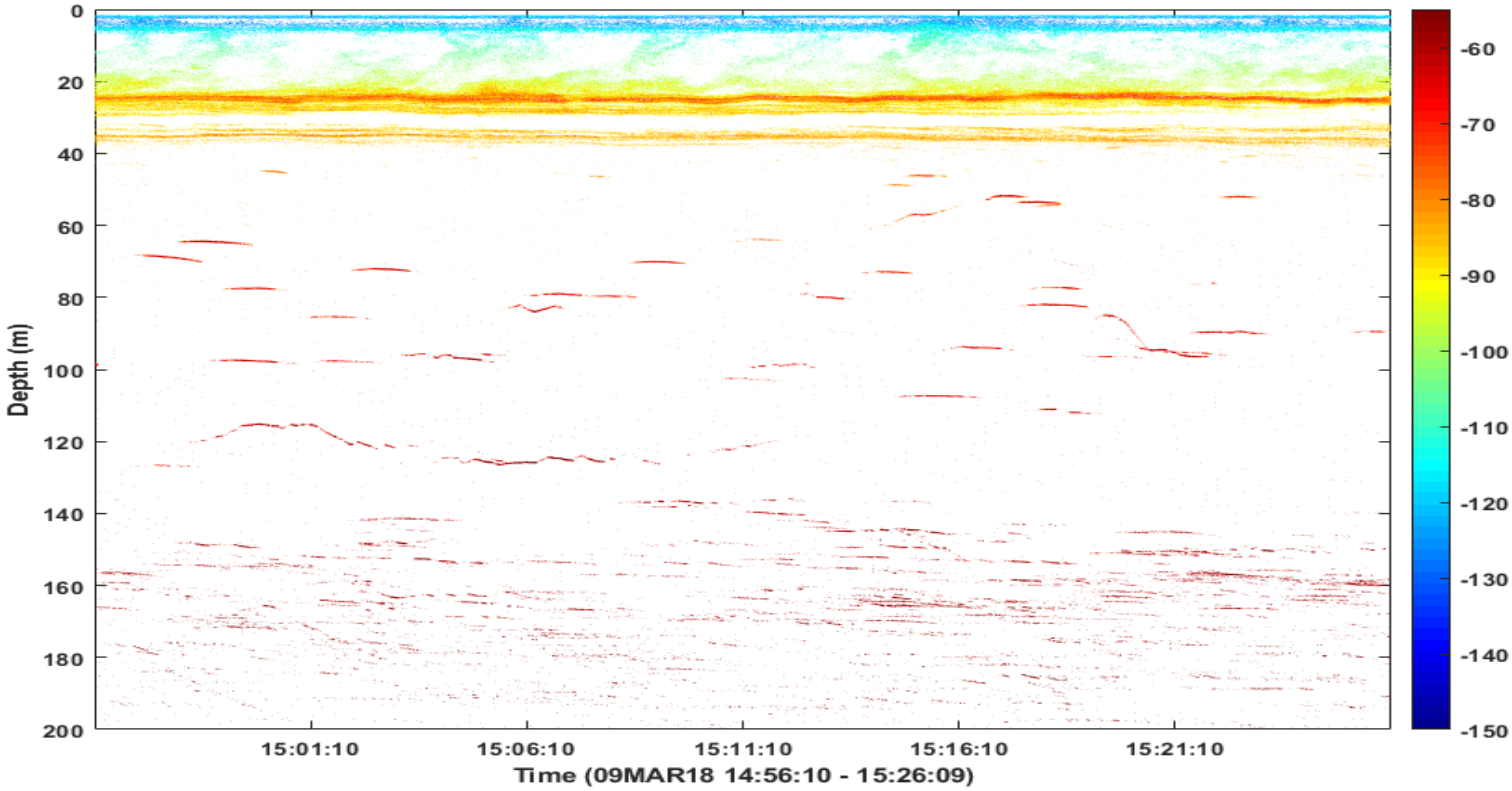

Note: The colorbar on the right represents EL in units of dB.

Figure 23. Fifth 30 Minutes of Noise-Removed 120-kHz Echosounder Data

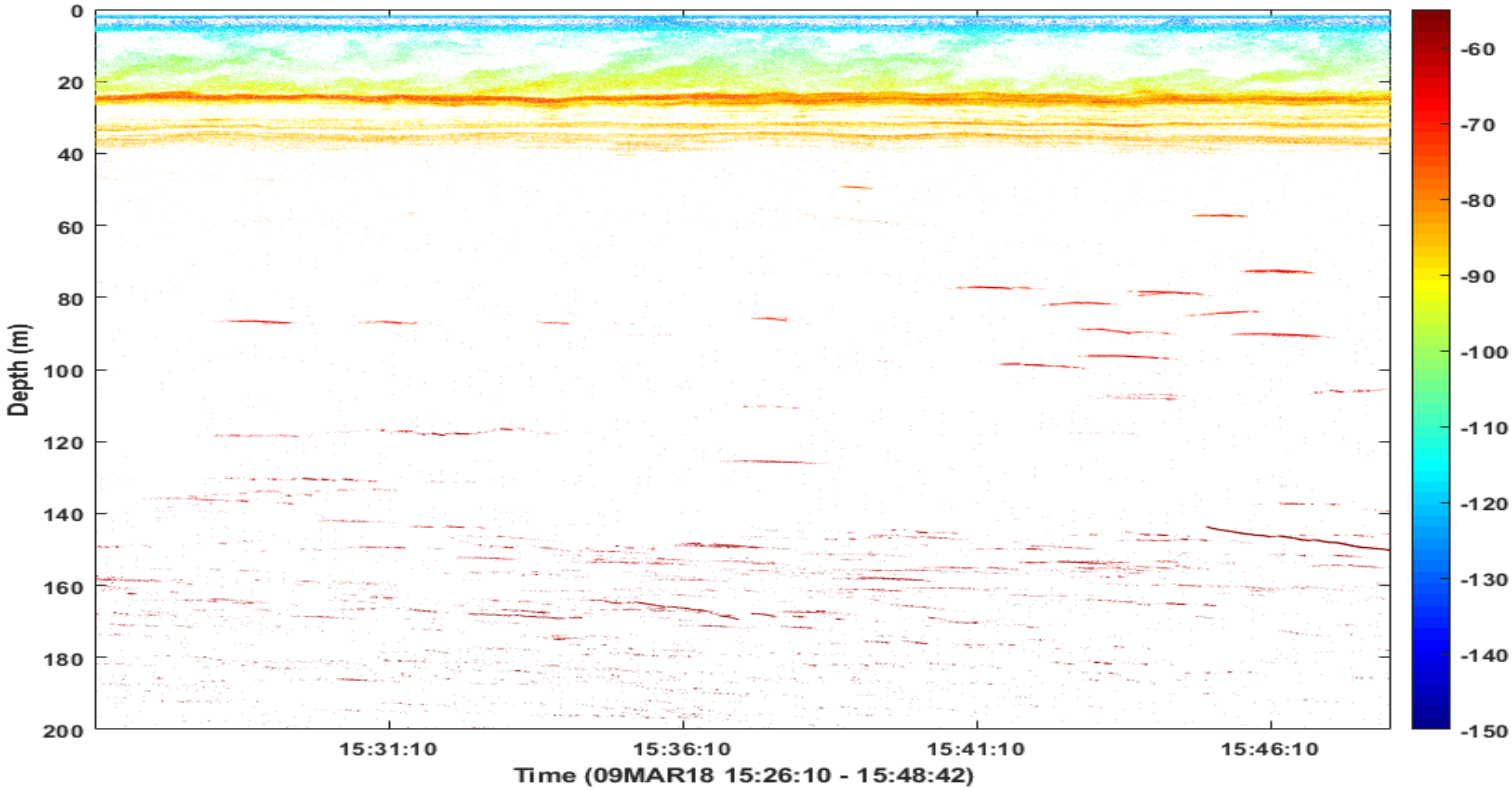

Note: The colorbar on the right represents EL in units of dB.

Figure 24. Final Minutes of Noise-Removed 120-kHz Echosounder Data

THIS PAGE INTENTIONALLY LEFT BLANK

LIST OF REFERENCES

Acoustimetrics, 2013: Acousonde 3A brochure. Accessed 09 January 2019, http://www.acousonde.com/downloads/Acousonde3A_Brochure.pdf.

Ashjian, C., 2004: Life in the Arctic Ocean. Woods Hole Oceanographic Institution, Accessed 26 January 2019, https://www.whoi.edu/oceanus/feature/life-in-the-arctic-ocean.

Baggeroer, A. B., H. Schmidt, and S. A. Carper, 2016: Detection and communication in the "Beaufort Lens." *J. Acoust. Soc. Amer.*, **140**, 4, 3408, https://doi.org/10.1121/1.4970950.

Bebieva, Y., and M.-L. Timmermans, 2017: The relationship between double-diffusive intrusions and staircases in the Arctic Ocean. *J. Phys. Oceanogr.*, **47**, 867–878, https://doi.org/10.1175/JPO-D-16-0265.1.

BioSonics, 2017: Visual Acquisition DT-X user guide: real-time data acquisition and playback software for BioSonics DT-X echosounder systems. Accessed 17 September 2018, https://www.biosonicsinc.com/products/software.

BioSonics, 2018: DT-X Extreme: Autonomous portable scientific echosounder. Accessed 28 January 2019, https://www.biosonicsinc.com/wp-content/uploads/2018/04/BioSonics-DT-X-Extreme-Spec-Sheet.pdf.

Cole, S. T., M.-L. Timmermans, J. M. Toole, R. A. Krishfield, and F. T. Thwaites, 2014: Ekman veering, internal waves, and turbulence observed under Artic sea ice. *J. Phys. Oceanogr.*, **44**, 1306–1328, https://doi.org/10.1175/JPO-D-12-0191.1.

Cushing, D. H., and I. D. Richardson, 1956: A record of plankton on the echo-sounder. *J. Mar. Biol. Ass. U.K.*, **35**, 231–240, https://doi.org/10.1017/S0025315400009085.

Davis, J. E., 2018: Effects of propagating submerged objects on diffusive staircases. M.S. thesis, Dept. of Physical Oceanography, Naval Postgraduate School, 51 pp., https://calhoun.nps.edu/handle/10945/59647.

DiMaggio, D., 2016: Observations and modeling of upper ocean hydrography in the Western Arctic with implications for acoustic propagation. Dissertation. Dept. of Physical Oceanography, Naval Postgraduate School, 143 pp., https://calhoun.nps.edu/handle/10945/51680.

Government of Canada, 2018: Magnetic field calculator. Accessed 14 December 2018, http://geomag.nrcan.gc.ca/calc/mfcal-en.php.

Hansen, W. J., and M. J. Dunbar, 1970: Biological causes of scattering layers in the Arctic Ocean. Proceedings, *Int. Symp. Biol. Sound Scattering in the Ocean*, Warrentown, VA, Maury Center for Ocean Science, 508–526.

Hansen, W., E. Bulleid, and M. J. Dunbar, 1971: Scattering layers, oxygen distribution and the copepod plankton in the upper 300 metres of the Beaufort Sea. McGill University Montreal Marine Sciences Centre. Note MS-20, 123 pp, https://apps.dtic.mil/dtic/tr/fulltext/u2/736684.pdf.

Holliday, D. V., and R. E. Pieper, 1980: Volume scattering strengths and zooplankton distributions at acoustic frequencies between 0.5 and 3 MHz. *J. Acoust. Soc. Amer.*, **67**, 1, 135–146, https://doi.org/10.1121/1.384472.

Jackson, J. M., E. C. Carmack, F. A. McLaughlin, S. C. Allen, and R. G. Ingram, 2010: Identification, characterization, and change of the near-surface temperature maximum in the Canada Basin, 1993–2008. *J. Geophys. Res.*, **115**, C05021, 1–16, https://doi.org/10.1029/2009JC005265.

Lavery, A. C., R. W. Schmitt, and T. K. Stanton, 2003: High-frequency acoustic scattering from turbulent oceanic microstructure: the importance of density fluctuations. *J. Acoust. Soc. Amer.*, **114**, 5, 2685–2697, https://doi.org/10.1121/1.1614258.

McBride, M. M., and Coauthors, 2014: Krill, climate, and contrasting future scenarios for Arctic and Antarctic fisheries. ICES J. Mar. Sci., 71, 7, 1934–1955, https://doi.org/10.1093/icesjms/fsu002.

McDougall, T. J., and P. M. Barker, 2011: Getting started with TEOS-10 and the Gibbs Seawater (GSW) Oceanographic Toolbox. Accessed 01 March 2019, www.teos-10.org/pubs/Getting_Started.pdf.

Meneghello, G., J. Marshall, J.-M. Campin, E. Doddridge, and M.-L. Timmermans, 2018: The ice-ocean governer: ice-ocean stress feedback limits Beaufort Gyre spin-up. *Geophys. Res. Lett.*, **45**, 11,293–11,299, https://doi.org/10.1029/2018GL080171.

Movable Type, 2018: Calculate distance, bearing and more between latitude/longitude points. Accessed 14 December 2018, https://www.movable-type.co.uk/scripts/latlong.html.

Nelson, M. S., 2016: Short-range acoustic propagation under Arctic ice cover during ICEX-16. M.S. thesis, Dept. of Physical Oceanography, Naval Postgraduate School, 55 pp., https://calhoun.nps.edu/handle/10945/50603.

Proni, J. R., and J. R. Apel, 1975: On the use of high-frequency acoustics for the study of internal waves and microstructure. *J. Geophys. Res.*, **80**, 9, 1147–1151, https://doi.org/10.1029/JC080i009p01147.

Radko, T., 2013: *Double-Diffusive Convection*. Cambridge University Press, 342 pp.

RBR, 2018: CT and CTD data loggers. Accessed 29 January 2019, http://rbr-global.com/wp-content/uploads/2018/06/0005579revB-RBRduo3-RBRconcerto3-datasheet.pdf.

Reeder D. B., J. M. Jech, and T. K. Stanton, 2004: Broadband acoustic backscatter and high-resolution morphology of fish: measurement and modeling. *J. Acoust. Soc. Amer.*, **116**, 2, 747–761, https://doi.org/10.1121/1.1648318.

Robinson, L. J., 2018: Statement of General Lori J. Robinson, United States Air Force Commander, United States Northern Command and North American Aerospace Defense Command before the Senate Armed Services Committee. U.S. Congress, Washington, DC, 20 pp, http://www.northcom.mil/Portals/28/Robinson_02-15-18%20SASC%20Testimony.pdf?ver=2018-02-15-105546-867.

Sea-Bird Scientific, 2006: SBE 19 SEACAT profiler CTD user's manual. Accessed 29 January 2019, https://www.seabird.com/cms-portals/seabird_com/cms/documents/discontinued-products/manual-sbe19.pdf.

Shibley, N. C., M.-L. Timmermans, J. R. Carpenter, and J. M. Toole, 2017: Spatial variability of the Arctic Ocean's double-diffusive staircase. *J. Geophys. Res.: Oceans*, **122**, 980–994, https://doi.org/10.1002/2016JC012419.

Simmonds, J., and D. MacLennan, 2005: *Fisheries Acoustics: Theory and Practice*. Blackwell Publishing, 437 pp.

Stranne, C., and Coauthors, 2017: Acoustic mapping of thermohaline staircases in the Arctic Ocean. *Sci. Rep.*, **7**, 15192, 1–9, https://doi.org/10.1038/s41598-017-15486-3.

Talley, L. D., G. L. Pickard, W. J. Emery, and J. H. Swift, 2011: *Descriptive Physical Oceanography: An Introduction*. Academic Press, 555 pp.

Teledyne Marine, 2009: Workhorse Sentinel: Self-contained 1200, 600, 300kHz ADCP. Accessed 28 January 2019, http://www.teledynemarine.com/Lists/Downloads/sentinel_datasheet_lr.pdf.

Timmermans, M.-L., and Coauthors, 2014: Mechanisms of Pacific Summer Water variability in the Arctic's Central Canada Basin. *J. Geophys. Res.: Oceans*, **119**, 7523–7548, https://doi.org/10.1002/2014JC010273.

Timmermans, M.-L., and S. R. Jayne, 2016: The Arctic Ocean spices up. *J. Phys. Oceanogr.*, **46**, 1277–1284, https://doi.org/10.1175/JPO-D-16-0027.1.

Trump, D. J., 2017: National Security Strategy of the United States of America. Washington, DC, 56 pp, https://www.whitehouse.gov/wp-content/uploads/2017/12/NSS-Final-12-18-2017-0905.pdf.

Turner, J. S., 1965: The coupled turbulent transports of salt and heat across a sharp density interface. *Int. J. Heat Mass Transfer*, **8**, 759–767, https://doi.org/10.1016/0017-9310(65)90022-0.

Turner, J. S., 2010: The melting of ice in the Arctic Ocean: the influence of double-diffusive transport of heat from below. *J. Phys. Oceanogr.*, **40**, 249–256, https://doi.org/10.1175/2009JPO4279.1.

Urick, R. J., 1983: *Principles of Underwater Sound*. Peninsula Publishing, 423 pp.

INITIAL DISTRIBUTION LIST

1. Defense Technical Information Center
   Ft. Belvoir, Virginia

2. Dudley Knox Library
   Naval Postgraduate School
   Monterey, California